

Understanding and Mitigating Membership Inference Risks of Neural Ordinary Differential Equations

Sanghyun Hong*
Oregon State University

Fan Wu
Arizona State University

Anthony Gruber
Sandia National
Laboratories

Kookjin Lee
Arizona State University

Abstract

Neural ordinary differential equations (NODEs) are an emerging paradigm in scientific computing for modeling dynamical systems. By accurately learning underlying dynamics in data in the form of differential equations, NODEs have been widely adopted in various domains, such as healthcare, finance, computer vision, and language modeling. However, there remains a limited understanding of the privacy implications of these fundamentally different models, particularly with regard to their membership inference risks.

In this work, we study the membership inference risks associated with NODEs. We first comprehensively evaluate NODEs against membership inference attacks. We show that NODEs are twice as resistant to these privacy attacks compared to conventional feedforward models such as ResNets. By analyzing the variance in membership risks across different NODE models, we identify the factors that contribute to their lower risks. We then demonstrate, both theoretically and empirically, that membership inference risks can be further mitigated by utilizing a stochastic variant of NODEs: Neural stochastic differential equations (NSDEs). We show that NSDEs are differentially-private (DP) learners that provide the same provable privacy guarantees as DP-SGD, the de-facto mechanism for training private models. NSDEs are also effective in mitigating existing membership inference attacks, demonstrating risks comparable to private models trained with DP-SGD while offering an improved privacy-utility trade-off. Moreover, we propose a drop-in-replacement strategy that efficiently integrates NSDEs into conventional feedforward models to enhance their privacy.

Keywords

Neural ODEs, Differential privacy, Membership inference

1 Introduction

In recent years, neural ordinary differential equations (NODEs) [10] have been gaining traction across various domains. This new family of neural networks enables modeling of underlying data distributions through learnable differential equations—a fundamental tool for describing processes in the physical world. By shifting from manually designing governing equations to data-driven modeling, NODEs have been deployed in various fields, such as time-series forecasting [10, 14, 36, 45, 56, 65, 75], scientific machine learning (ML) [29, 30, 49, 64, 71, 84], or general ML tasks [10–12, 17, 68, 78, 80]. Moreover, applications of NODEs in finance or healthcare [34, 48, 65], which heavily rely on time-series or physics-informed modeling, are becoming closely integrated into our daily lives.

Since NODEs are deployed in fields where the training data often contains confidential or sensitive information, such as patient medical records from hospitals, this naturally raises privacy concerns. Recent work has shown the risk of membership inference [66], where an adversary can determine if a specific data record was part of the training set. Membership inference has been extensively studied in the context of feedforward neural networks, such as convolutional neural networks [5, 66, 67, 79] or Transformer-based language models [82]. However, this risk has not been studied against NODEs that operate differently, with their internal structures designed based on principles from mathematical modeling. It is unclear whether applications using these models face similar privacy risks, and how to mitigate them while preserving usability.

In this work, we study the privacy implications of employing differential equation-based neural networks, such as NODEs. Specifically, we address the following four research questions:

① *How vulnerable are NODEs to membership inference attacks?* We address this question empirically through a systematic evaluation. We implement a risk analysis framework that runs five off-the-shelf membership inference attacks across a variety of neural networks including NODEs and baseline feedforward models. In evaluation on two datasets (CIFAR-10 and CIFAR-100), commonly used in prior work on assessing membership risks, we demonstrate that NODEs exhibit up to $2\times$ lower membership risks compared to feedforward neural networks, like ResNets [32]. We also find that this is partly due to NODEs exhibiting less overfitting while achieving accuracy comparable to conventional neural network models.

Moreover, we analyze factors that may contribute to this membership risks. We first examine configurations one can control at the block-level: solvers, tolerance, and step size. Our analysis indicates that these factors, which affect the complexity of learned dynamics while keeping the same model capacity, can increase/decrease the likelihood of overfitting. We also test the model-level configurations: the number of blocks and advanced variants of NODEs [17, 59, 78]. They increase the model capacity or the complexity of learned dynamics, and therefore, increase membership risks.

② *How can we mitigate the membership risks of NODEs?* Our previous evaluation shows that while NODEs are less vulnerable, the risks to membership inference still exist. We next address this problem by focusing on a stochastic adaptation of NODEs: neural stochastic differential equations (NSDEs) [53]. NSDEs, similar to NODEs, model the underlying dynamics with ODEs but augment them with a diffusion term that incorporates Gaussian noise.

We first formally show that this diffusion term functions as a differentially-private (DP) mechanism during training, and therefore, NSDEs become DP-learners. We establish a theoretical bound on the privacy leakage of NSDEs at each iteration of mini-batch SGD and then present a mechanism for accounting for the total

*Corresponding author.

privacy leakage during training. Surprisingly, we show that the total privacy leakage (ϵ) guaranteed by the NSDE training process is the same as that of the de-facto standard for training private models, DP-SGD [1]. The leakage ϵ is proportional to the number of training iterations and the level of the Gaussian noise (σ).

We then empirically evaluate the effectiveness of NSDEs in further reducing the membership inference risks. We demonstrate that NSDEs can make existing membership inference attacks 1.8–10× less effective compared to their effectiveness on NODEs. We observe that the utility of those NSDE models, under the same privacy guarantees, is comparable to (or slightly higher than) that of ResNet models trained with DP-SGD. This shows their potential as a countermeasure with an improved privacy-utility trade-off. We also compare NSDEs with heuristic defenses [41] designed to counter membership inference attacks but lacking provable privacy guarantees. We show that NSDEs are 2–5× more effective in mitigating the membership inference risks.

Q3 *How can existing pre-trained models be augmented with NSDEs to enhance privacy?* Implementing our privacy mechanism requires training a new NSDE model from scratch, which can be a computationally demanding option for service providers. We address this practical challenge by efficiently applying NSDEs to existing pre-trained models, particularly conventional feedforward models like ResNets. We leverage the common practice of *transfer learning* in supervised learning, where the last layer of a pre-trained model are replaced with a classification head, followed by fine-tuning on data over a few iterations. Our strategy, *replace-then-finetune*, replaces the last few layers of a pre-trained model with an NSDE block. We test our strategy on ResNet14 pre-trained on CIFAR-10. Our evaluation shows that fine-tuned models achieve accuracy comparable to the pre-trained models, while reducing the membership risks by 10× in CIFAR-10. We hope our work encourages the adoption of NSDEs as a viable mechanism for further reducing privacy risks while maintaining model utility.

Contributions. In summary, our contributions are:

- We are the first to study the membership inference risks of NODEs, which utilize a fundamentally different approach to modeling data distributions. Our comprehensive evaluation shows that NODEs exhibit 2× lower membership risks compared to feedforward neural networks like ResNets. We also analyze the factors contributing to this reduced risk.
- We propose NSDEs as a defensive mechanism for mitigating the membership inference risks of NODEs. We formally show that NSDEs are DP learners, offering the same provable privacy guarantees as DP-SGD. We also present an accounting mechanism to track the total privacy leakage during NSDE training.
- We show, in our empirical evaluation that NSDEs achieve a 2–5× reduction in membership risks compared to defenses without provable guarantees applied to NODEs. Compared to private models trained with DP-SGD, NSDEs demonstrate the same effectiveness in mitigating membership inference attacks while achieving slightly higher accuracy.

- We present a practical strategy to leverage this privacy benefit without fully replacing existing models with NSDEs, *replace-then-finetune*. It reduces membership risks by 10× while achieving a higher utility than the models trained with DP-SGD.

2 Background

2.1 Neural Ordinary Differential Equations

NODEs model the dynamics of system states as a system of ODEs such that:

$$\frac{d\mathbf{h}(t)}{dt} = \mathbf{f}_{\Theta}(\mathbf{h}(t), t),$$

where $\mathbf{h}(t)$ are the state variables and \mathbf{f}_{Θ} is a neural network, parameterized by its parameters Θ , defining the rate of change in $\mathbf{h}(t)$. The scalar variable t typically refers to a time variable and the system states correspond to observables in time-dependent physical processes [69] or measurements in time-series data (e.g., [65]). However, in the context of hidden representations within a deep feedforward network (FFN), t instead refers to a continuous depth parameter. More precisely, recall that the flow map $\varphi = \varphi(t, \mathbf{h})$ of an ODE system associates to each state \mathbf{h} its “flowed out” state after evolving along the ODE for t time, i.e., $\varphi(0, \mathbf{h}) = \mathbf{h}$ and $(d/dt)\varphi(t, \mathbf{h}) = \mathbf{f}_{\Theta}(\mathbf{h}(t), t)$ in the case of the NODE above. Then, the number of “layers” in the NODE architecture defined by \mathbf{f}_{Θ} is analogous to the number of “time steps” used to generate the flowed-out state $\mathbf{h}(t)$, and hence each network prediction based on this quantity. Our focus is on this use case, which allows for depth control through direct manipulation of the ODE time-stepping.

Training and inference. In NODEs, the forward pass involves solving an initial value problem (IVP) describing the evolution of some given initial states under the flow of the learnable ODE in question. Given an initial condition $\mathbf{h}(0) = \mathbf{h}_0$ for the state variables (or hidden state representations), the states at any time index $\{\mathbf{h}(t_i)\}_{i=1}^n$ can be obtained by solving the associated IVP, lending NODEs their interpretation as continuous-depth FFNs. To solve the necessary IVP, a black-box ODE time-integrator with solver options OPT can be employed:

$$\mathbf{h}(t_1), \dots, \mathbf{h}(t_n) = \text{ODESolve}(\mathbf{f}_{\Theta}, \mathbf{h}(0), [t_1, \dots, t_n], \text{OPT}).$$

Different choices of numerical time-integration yield different realizations of FNNs, e.g., under the forward Euler method with step size 1, autonomous (t -independent) NODEs degenerate to ResNets [32], $\mathbf{h}(t_{i+1}) = \mathbf{h}(t_i) + \mathbf{f}_{\Theta}(\mathbf{h}(t_i))$. With this setup, the forward pass for both training and inference is equivalent to recurrently applying a nonlinear transformation, defined by \mathbf{f}_{Θ} , to a hidden state, followed by a skip connection. In classification tasks, the last hidden representation $\mathbf{h}(t_n)$ is fed into a classifier network, producing logits, and the loss of the model is obtained via computing the cross-entropy. The continuous-depth network $\mathcal{M}(t, \mathbf{h}) = \mathcal{M}_t(\mathbf{h})$ can then be thought of as discretizing the ODE flow map, i.e., $\mathcal{M}_{t_n}(\mathbf{h}_0) = \mathbf{h}(t_n)$, where $\mathbf{h}(t_n)$ is the solution of the IVP defined above. As mentioned before, any intermediate time steps t_1, \dots, t_{n-1} used in the production of the final state $\mathbf{h}(t_n)$ are analogous to the labels on hidden layers in an FFN.

For the backward process required during training, NODEs use either standard backpropagation through the rolled-out computational path, or the adjoint sensitivity method [63]. The primary

challenge lies in achieving stable and memory-efficient gradient computation for \mathbf{f}_{Θ} with respect to its parameters, as backpropagating directly through an iterative numerical solver can be memory intensive and exacerbate vanishing or exploding gradient issues.

NODE variants. Many variants have been developed to improve their expressivity and efficiency. Augmented NODEs (ANODEs) [18] propose an additional dimension to the state variable $[\mathbf{h}(t), \mathbf{a}(t)]$, to increase expressivity. ANODEs were further extended into second-order NODEs (SONODEs) [59], which formulates a system of coupled first-order NODEs, implementing the broader class of augmented models. Other variants incorporate concepts from gradient descent optimization, such as momentum, resulting in heavy ball NODEs (HBNODEs) [78] and Nesterov NODEs [58], both of which improve computational efficiency by reducing the number of function evaluations in the forward pass.

NSDEs [43, 51, 53] extend NODEs to the modeling of stochastic processes, typically introducing randomness in the form of additive Gaussian noise. These systems can be formulated in terms of deterministic, vector-valued “drift” and stochastic, matrix-valued “diffusion” terms as follows:

$$d\mathbf{h} = \mathbf{f}_{\Theta_1}(\mathbf{h}, t) dt + \mathbf{G}_{\Theta_2}(\mathbf{h}, t) d\mathbf{B}_t,$$

where $d\mathbf{B}_t$ denotes the Wiener increment—a zero mean, unit variance, delta-correlated Gaussian process describing “white noise”. A simple but popular discretization of NSDEs is given by the Euler–Maruyama method [61] with step size 1, expressed as $\mathbf{h}(t_{i+1}) = \mathbf{h}(t_i) + \mathbf{f}_{\Theta_1}(\mathbf{h}, t_i)\Delta t + \mathbf{G}_{\Theta_2}(\mathbf{h}, t_i)\mathbf{w}_{t_i}$, where Δt is the time step size and $\mathbf{w}_{t_i} \sim \mathcal{N}(0, \Delta t)$ is randomly sampled. In this formulation, Gaussian noise is injected alongside each residual connection. Because of this property, NSDEs have shown enhanced robustness against adversarial examples [54] compared to standard NODEs. Our study further explores this property as a formal mechanism for mitigating privacy risks.

2.2 Membership Inference Attacks

Membership inference attacks aim to determine whether a specific example is a *member* of the training data. To do this, the attacker exploits the difference in the target model’s response to the specific example when it is a member versus a non-member. Membership inference can be considered a threat on its own, but a model’s vulnerability to inference attacks also implies its potential to leak other private information outside of this context, an idea which aligns closely with the definition of differential privacy [19] as a worst-case certification.

Existing attacks. Prior work has developed various attacks to exploit differences and identify *membership*. In our work, we evaluate NODEs against each of the representative attacks described below:

- Yeom *et al.* [79] formulate an attack which focuses on differences in *loss* values: for a specific example $z = (x, y)$, a model will be more accurate in its predictions when it has seen z during training. The attack predicts z as a member if and only if, for a threshold τ , the model’s loss on z is below τ ; otherwise, it is classified as a non-member.
- Shokri *et al.* [66] attack based on *shadow models* which better approximate the differences in a model’s responses to members versus non-members. When constructing shadow models, the

attacker artificially generates datasets for training and testing these models so that the members and non-members are known in advance. The attacker collects responses from shadow models for both members and non-members and trains a classifier to predict membership of z based on the target model’s response.

- Song and Mittal [67] leverage the *prediction correctness* to compute the threshold τ for identifying membership. Instead of training classifiers to perform attacks, τ is designed such that correct predictions with high confidence yield the lowest values while confident but incorrect predictions achieve the highest.
- Watson *et al.* [73] proposed *per-example difficulty* calibration in which an attacker leverages shadow models trained without a particular example to compute the average confidence level of a model. The average is then subtracted from the example’s confidence obtained from the target model to calibrate the difficulty of the sample.
- Carlini *et al.* [5] introduced the Likelihood Ratio Attack (LiRA), which carefully controls how the adversary splits shadow training data. For each sample in the shadow training data, LiRA trains two sets of shadow models: models with the sample included (“in”) and the others without (“out”). The attacker then collects logits from both members and non-members across these shadow models, computes the threshold (or LiRA membership score) as the ratio of the likelihoods of observing the logit for the sample z in the “in” versus “out” models, and uses this score to identify membership.

Metrics. Initial work [79] on membership inference uses inference accuracy as a metric for evaluating attack success. Subsequent works also use the area under the ROC curve (AUC) as an additional metric to report the balance between true-positive (TPR) and false-positive rates (FPR). Recent work by Carlini [5] proposes evaluating attack success in a worst-case *low-FPR regime*. Our work employs all these metrics in evaluation.

2.3 Defenses against Membership Inference

Prior work has developed defenses to obscure the difference in model output between members and non-members.

Reducing overfitting. One key difference is the degree of overfitting or the extent to which a model memorizes its training data. Yeom *et al.* [79] found that defending against membership inference attacks and reducing overfitting go hand-in-hand, so that the goals of privacy and performance are aligned. Many defenses [38, 66, 67] therefore focus on a regularization effect, and existing regularization methods are also being used to reduce membership risk [41].

- ℓ^p -regularization and dropout are two of the most commonly used regularization techniques in practice, shown effective against membership inference attacks [66].
- *Early stopping* is a straightforward way to prevent overfitting [67]. One halts training when the model’s performance stops improving. This has the effect of stopping the model before it can begin to memorize.
- *MMD with Mix-up* [50] combines two different mechanisms: (1) a maximum mean discrepancy (MMD) loss to reduce the training accuracy to match validation accuracy, and (2) training on mix-up augmented data, where a linear interpolation between two

randomly drawn examples (and their labels) is used instead of individual samples. Mix-up has been shown to increase overall accuracy and further reduce overfitting.

- *MemGuard* [38] uses an “attack-as-a-defense” approach: It adds carefully-calibrated noise to each confidence score vector predicted by the target model. Once added, the resulting adversarial examples mislead the attacker’s membership identification (e.g., the attack classifiers).

Differential privacy [19] (DP) is a mathematical framework that provides a probabilistic privacy guarantee. Precisely, the following definition implies that, as a random variable, the privacy loss is bounded in the worst case by a constant $\epsilon > 0$ with probability $0 < 1 - \delta < 1$.

Definition 2.1 ((ϵ, δ)-Differential Privacy). Given any two datasets D and D' that differ by only a single record, a mechanism M satisfies (ϵ, δ)-DP if, for any subset S of the image of M ,

$$\Pr[M(D) \in S] \leq e^\epsilon \Pr[M(D') \in S] + \delta$$

where ϵ is the privacy budget (or leakage) and δ is the failure probability.

A primary advantage of DP is its immunity to post-processing: an (ϵ, δ)-DP algorithm cannot be weakened through manipulation of its output. Based on this property, Abadi *et al.* proposed an effective, differentially-private adaptation of stochastic gradient descent: DP-SGD [1]. The key in DP-SGD is the *moment accountant*, a mechanism that tracks total privacy leakage possible under a worst-case adversary. This leakage is typically denoted as ϵ , a convention that will be followed throughout the rest of the paper. Because of the formal privacy guarantee that DP-SGD offers, it has become a de-facto standard for constructing private models. However, this approach inherently leads to a utility loss due to the addition of Gaussian noise to the gradients required for accurate learning.

We evaluate how effective those defenses are in mitigating the membership risks of NODEs and formally demonstrate that NSDEs are DP learners, offering an improved privacy-utility tradeoff.

3 Membership Risks of NODEs

We first evaluate the membership risks of NODEs. Our hypothesis is that these models are vulnerable to existing membership inference attacks as their performance on popular benchmarking tasks is comparable to conventional feedforward networks. However, because of their expressivity limited to modeling a system of ODEs, the risk could be lower than that of conventional networks.

3.1 Threat Model

The attacker aims to determine whether a specific sample $z = (x, y)$ is included in the data used for training the target model f . The adversary only has *black-box* access to f .¹ We assume that the attacker can train shadow models f_s with known membership for all shadow training samples and use them to infer membership from the model output. Because the attacker aims for f_s to closely resemble the behaviors of f , we assume the attacker’s shadow training dataset and the original training data come from the same

¹Nasr *et al.* [57] showed that a *white-box* membership adversary with full access to the model and its parameters, does not particularly perform better than black-box attacks.

underlying data distribution and may overlap partially. We also assume a worst-case black-box adversary with full knowledge of f ’s architecture and training configurations such that they employ this knowledge to construct and train f_s . When evaluating defenses in Sec 5, we consider an *adaptive* adversary who knows the defense mechanisms deployed on f and their hyper-parameters.

3.2 Experimental Setup

Datasets. We use CIFAR-10 and CIFAR-100 [47], which are object recognition benchmarks, composed of 32×32-pixel RGB images over 10 and 100 object classes, respectively. These datasets are commonly employed in prior work [5, 66, 68, 79]. We employ them to evaluate and compare the membership risks of NODEs with those reported in prior studies on feedforward neural networks.

Models. For each dataset, we train models with architectures based on one studied in Oganessian *et al.* [60]. They have a first few convolutional layer for downsampling, followed by three residual or ODE blocks (see Appendix A for details). For our baseline, we use a ResNet architecture (**ResNet-14**) with 3 residual blocks where each block within a group has the same size and each group has 16, 32, and 64 filters respectively, widened by a factor of 2. Our NODEs substitute an ODE block for each group of residual blocks. **ODENet-16-32-64** has the same dimensions. We also examine **ODENet-64**, which contains only one ODE block after the downsampling layers—a typical structure used in prior work [10, 17].

Metrics. Following best practices from prior work [5], we measure the membership risks by computing the true-positive rate at a low false-positive rate (*TPR@0.1–1% FPR*). We also compare *AUC* and inference accuracy (or *accuracy*). Because this empirical membership risk is highly connected to a model’s generalization gap, we report both the best train and test accuracies of target models.

3.3 Quantifying the Membership Risks

Methodology. We evaluate our models against five membership inference attacks outlined in Sec 2.2. For the attacks employing shadow models, we train 16 models on 16 different subsets of the original training dataset. Following the strategy of prior work [5], we construct these 16 different shadow training datasets such that each training sample is included in half of the sets and excluded from the other half. We then choose one of them as the target model f and the remaining 15 as shadow models f_s . We run 16-fold cross-validation by choosing a different target model from the 16 models in each round, and we report the averaged metrics. For attacks like those by Yeom *et al.*, which do not use shadow models.

Results. Table 1 summarizes our results. Due to the page limit, we include the ODENet-64 results in Appendix C and compare ResNet-14 and ODENet-16-32-64. We first observe that *NODEs exhibit reduced overfitting*. To quantify overfitting, we compare the difference between training and testing accuracy. To achieve a comparable test accuracy 84–86% on CIFAR-10, NODEs achieve a training accuracy of 94.3% (+9.1%), while ResNet-14 attains 98.1% (+12.1%). On a more complex task like CIFAR-100, ResNet-14 shows a difference of 24.6%, compared to 15.8% for NODEs.

Next, we compare the membership risks of NODEs and ResNet-14 models. We observe in overall, *NODEs is twice less vulnerable to membership inference attacks*, compared to ResNet14, on both

Table 1: Comparison of membership inference risks. We evaluate two different types of neural networks against five existing attacks on CIFAR-10 and CIFAR-100. We compare their risks based on four different metrics used in the prior work.

Model	Method	Acc. (C-10)		Acc. (C-100)		TPR @ 0.1% FPR		TPR @ 1% FPR		AUC		Inference acc.	
		Train	Test	Train	Test	C-10	C-100	C-10	C-100	C-10	C-100	C-10	C-100
ResNet-14	Yeom et al. [79]					0.00%	0.00%	0.00%	0.69%	0.590	0.767	58.92%	73.81%
	Shokri et al. [66]					0.01%	0.01%	0.14%	0.06%	0.411	0.336	50.00%	50.00%
	Song and Mittal [68]	98.1%	86.0%	94.99%	54.26%	0.00%	0.25%	0.00%	1.76%	0.590	0.494	58.92%	51.19%
	Watson et al. [73]					0.00%	0.00%	0.00%	0.62%	0.590	0.767	58.92%	73.81%
	Carlini et al. [5]					3.96%	10.52%	10.57%	25.95%	0.679	0.865	61.15%	76.46%
NODE (ODENet-16-32-64)	Yeom et al. [79]					0.00%	0.01%	0.00%	0.71%	0.558	0.701	56.59%	70.75%
	Shokri et al. [66]					0.04%	0.04%	0.43%	0.37%	0.448	0.398	50.01%	50.00%
	Song and Mittal [68]	94.3%	84.4%	82.05%	52.16%	0.00%	0.15%	0.00%	1.66%	0.529	0.498	54.22%	52.48%
	Watson et al. [73]					0.00%	0.01%	0.00%	0.71%	0.558	0.701	56.69%	70.75%
	Carlini et al. [5]					1.01%	3.30%	4.22%	12.11%	0.616	0.782	57.65%	72.88%

CIFAR-10 and CIFAR-100. In most cases on CIFAR-10, attacks other than that by Carlini *et al.* show a TPR of $\sim 0.0\%$ at 0.1% or 1.0% FPR. The attack by Carlini *et al.* (LiRA) is 2.5–4 \times times less effective on NODEs than ResNet-14. On CIFAR-100, the other attacks also show some effectiveness, with TPRs of up to 1.5%, but the LiRA attack remains the most effective. LiRA shows similar effectiveness in at 0.1% FPR, but 1.4 \times less effective at 1% FPR. We make the same observations from AUC and inference accuracy.

However, our results do not imply that NODEs are free from membership risks. The attacks are still effective, with TPRs ranging from 1.1% to 10.6% at low FPRs across the two datasets.

Generalization gap is a known factor contributing to membership risks. Previous studies [66, 79] indicate that risks increase when a model *overfits*—it shows a large disparity between the training and testing accuracy. Hence, we analyze whether our results of the reduced membership risks of NODEs is because of overfitting.

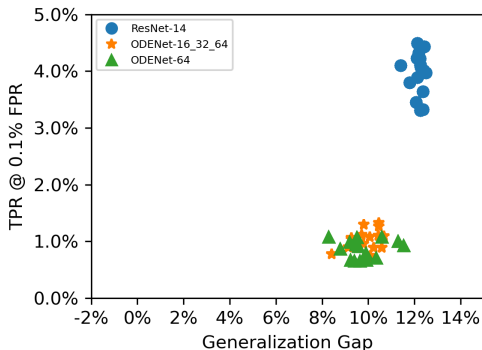
**Figure 1: Membership risks and overfitting in CIFAR-10.**

Figure 1 shows the interaction between membership risks and the generalization gap in CIFAR-10. We plot the attack success and the generalization gap observed for each of the 16 target models, considering LiRA [5], the strongest known attack. Overall, we observe that overfitting has no significant impact on the success of membership inference attacks. In ResNets, the TPR @ 0.1% FPR fluctuates between 3–5% while the generalization gap remains $\sim 12\%$. NODE models (ODENet-16_32_64 and -64), with 0.5–1.5% TPR @

0.1% FPR, show the generalization gap in 8–12%. Please refer to Appendix C for our results in CIFAR-100.

3.4 Characterizing the Membership Risks

We now run an in-depth analysis of the factors that may attribute to the membership risks. We first examine the choice of ODE solvers (a block-level configurations) and then analyze model-level factors: the number of ODE blocks and the choice of equations used for modeling a system. Figure 2 summarizes our results.

Impact of a solver. In all our experiments, we use Euler’s method as the default solver; but, other popular choices exist in the literature. We therefore analyze how the choice of solver impacts the membership risks of NODEs. We train and test the same NODEs with two other solvers: a fixed-step solver, Runge–Kutta (RK4) [4] and an adaptive-step solver, Dormand–Prince (Dopri5) [16].

The leftmost figure illustrates the success rate of LiRA on NODEs trained and tested with three different solvers. Overall, we observe a marginal difference in attack success across these models. In both CIFAR-10 and CIFAR-100 (shown in Appendix C), the TPR remains 0.7–1.0% and 3.0–3.3% @ 0.1% FPR, respectively. Upon closer examination, Euler and RK4 yield similar risks, while Dopri5 shows $\sim 0.3\%$ lower TPR at the same FPR. We attribute this to Dopri5’s use of adaptive step-sizes. During the training of a NODE model with Dopri5, it stops processing of an input when the error rate becomes sufficiently small—within the predefined tolerance value. It acts as an early-stopping mechanism [67], preventing the model from becoming overconfident on specific training samples. On the other hand, RK4, by modeling data with higher-order polynomials may achieve an increased training (and testing) accuracy. However, the ability to perform complex modeling can introduce a risk of overfitting to specific training samples, which can also increase membership inference risks. In CIFAR-100, a more complex task than CIFAR-10, we observe 0.3% and 1.0% higher TPR at 0.1% and 1% FPR, respectively, compared to the model using Euler.

Impact of the number of ODE blocks. Our NODEs replace a group of residual blocks with an ODE block, a configuration chosen for its comparable accuracy to ResNet models. But we can increase

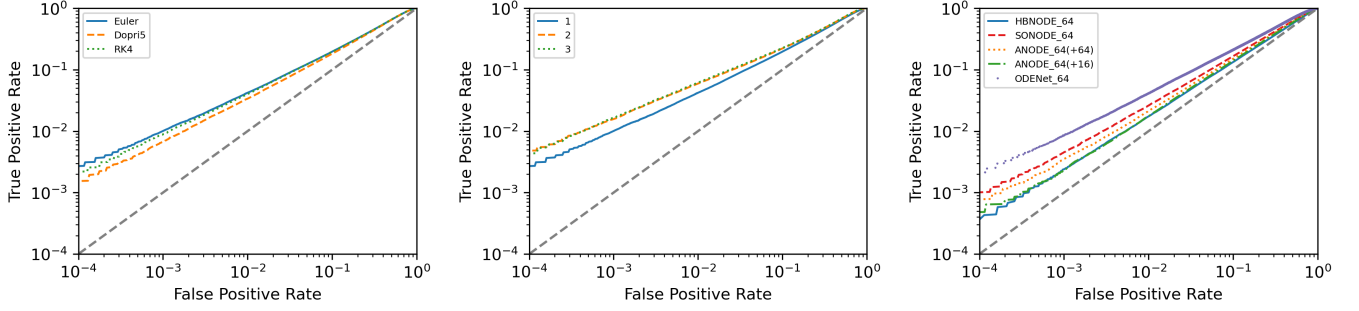


Figure 2: Characterization of membership risks in NODEs with different configurations. We vary the choice of ODE solvers (left), the number of ODE blocks (middle), and the equations used for modeling a system (right). We show the results in CIFAR-10 against LiRA [5], the strongest membership inference attack. Please refer to Appendix for details and results in CIFAR-100.

the number of blocks further. We hypothesize that, because additional ODE blocks enhance the model’s ability to represent complex systems, this may lead to an increase in membership risks.

The middle figure shows the membership risks of NODEs when the number of ODE blocks is increased from 1 to 3. We observe that increasing the number of ODE blocks leads to higher membership risks. This is primarily because more parameters increase the likelihood of *overfitting*. However, we do not observe significant performance gains from the decision, meaning that simply adding blocks is not an ideal strategy for improving the performance.

Non-stochastic NODE variants. In Sec. 2.1, we review NODE variants designed to enhance expressivity and stability, ultimately improving generalization. We examine whether these benefits come with a reduction in membership risks. We evaluate ANODE [17], SONODE [59] and HBNODE [78]. ANODE introduces additional dimensions to NODEs, and SONODE extends the modeling equations to second order, while HBNODE incorporates momentum into the system equations, stabilizing the ODEs learned by the model. We select ODENet-64 as our baseline model because it is composed of a single ODE block, making it easy to extend to NODE variants. We implement SONODE and HBNODE using an ODE block identical to that in ODENet-64. We augment ODENet-64 with an additional 16 and 64 dimensions (ANODE). These variants are expected to enhance the model’s generalization capabilities, allowing us to assess the impact of better system modeling on membership risks.

The rightmost figure compares the membership risks of these models with those of the baseline ODENet-64 model. We first observe that NODE variants, except for the HBNODE model, achieves higher test accuracy (84.6%–86.5%) than the baseline (84.4%). SONODE performs the best with 86.5%, followed by ANODE (+64) at 85.1% and ANODE (+16) at 84.6%. But HBNODE achieves 82.1%. Interestingly, we find that *all the NODE variants are less vulnerable to LiRA*. SONODE, ANODE (+64), ANODE (+16), and HBNODE achieve TPRs of 0.44%, 0.35%, 0.24%, and 0.24% at 0.1% FPR, respectively, compared to ODENet-64 with a TPR of 0.86% at 0.1% FPR. We attribute this to the reduced overfitting shown by NODE variants. The differences between training and testing accuracy are 5.9%, 4.0%, 3.0%, and 2.8% for SONODE, ANODE (+64), ANODE (+16), and HBNODE, respectively, compared to 9.7% gap in ODENet-64. However, for HBNODE, there is a possibility that the lower risk

is attributed to the lack of generalization. Modeling NODEs with momentum (HBNODE) enhances the stability, but does not increase a model’s capacity. In our evaluation, the training accuracy of HBNODE is 84.9%, 2.8–7% lower than that of the other variants.

4 NSDEs Are DP-Learners

In the previous section, we demonstrated that NODEs and their non-stochastic variants are still vulnerable to membership inference attacks. We now shift our focus to the stochastic variants of NODEs, particularly neural stochastic differential equations (NSDEs) [54]. In NSDEs, which contain “drift” and “diffusion” terms, stochasticity arises from the *randomness in the diffusion term*, typically modeled as white or colored Gaussian noise. We hypothesize that this diffusion term leads NSDEs to function as a differentially-private (DP) mechanism [19], preserving the privacy of its inputs along its evolution. Here we first formally show that NSDEs are DP-learners. Because of the diffusion term, those models learn “differentially-private” systems of ODEs, achieving privacy without the need of additional mechanisms, such as DP-SGD [1], which alters the training process. Next in Sec 5, we empirically assess the membership risks of NSDEs in comparison to non-stochastic NODE variants and “private” feedforward models trained with DP-SGD.

4.1 Theoretical Analysis

NSDEs model the dynamics of system states as:

$$d\mathbf{h} = \mathbf{f}(\mathbf{h}, t) dt + \mathbf{G}(\mathbf{h}, t) d\mathbf{B}_t,$$

in terms of a drift function $\mathbf{f} : \Omega \rightarrow \mathbb{R}^n$ and a diffusion term $\mathbf{G} : \Omega \rightarrow \mathbb{R}^{n \times n}$, where the explicit dependence on parameters Θ has been dropped for notational convenience. Our privacy bounds will make use of the *sensitivity* of a function $\mathbf{g} : \Omega \rightarrow \mathbb{R}^n$ (c.f. [19]):

$$S_{\mathbf{g}} = \max_{\|\mathbf{h} - \mathbf{h}'\| \leq 1} |\mathbf{g}(\mathbf{h}) - \mathbf{g}(\mathbf{h}')|.$$

Here, we adopt the following natural assumptions from the work by Liu *et al.* [54], which guarantees the well-posedness of the SDE formulation under consideration.

ASSUMPTION 1 (SUBLINEAR GROWTH). \mathbf{f} and \mathbf{G} grow at most linearly, i.e., there exists a constant $c > 0$ such that $|\mathbf{f}(\mathbf{h}, t)| + |\mathbf{G}(\mathbf{h}, t)| \leq c(1 + \|\mathbf{h}\|)$ for all $\mathbf{h} \in \Omega$ and $t \geq 0$.

ASSUMPTION 2 (LIPSCHITZ CONTINUITY). \mathbf{f} and \mathbf{G} are L -Lipschitz, i.e., there exists a constant $L > 0$ such that $|\mathbf{f}(\mathbf{h}, t) - \mathbf{f}(\mathbf{h}', t)| + |\mathbf{G}(\mathbf{h}, t) - \mathbf{G}(\mathbf{h}', t)| \leq L|\mathbf{h} - \mathbf{h}'|$ for all $\mathbf{h}, \mathbf{h}' \in \Omega$ and $t \geq 0$.

With these conditions in place, the following theorem establishes the differential privacy of the SDE mechanism.

THEOREM 4.1 (SDEs ARE DIFFERENTIALLY-PRIVATE). Suppose $\sigma, T > 0$ and $\mathbf{f}(\mathbf{h}, t) : \Omega \rightarrow \mathbb{R}^n$ is Lipschitz-continuous with constant $L_{\mathbf{f}}$. Consider the well-posed SDE:

$$d\mathbf{h} = \mathbf{f}(\mathbf{h}, t) dt + \frac{\sigma}{\sqrt{T}} d\mathbf{B}_t.$$

For any privacy budget $0 < \epsilon < 1$ and failure probability $\delta > 0$, the mechanism $\mathbf{M}(\mathbf{h}) = \mathbf{h}(T)$, defined by the flow map of the SDE at time T , is (ϵ, δ) -differentially private, provided that $\sigma \geq \sqrt{2 \ln(1.25/\delta)}(TL_{\mathbf{f}}/\epsilon)^2$.

PROOF. Recall that the Wiener increment $d\mathbf{B}_t$ satisfies $\int_s^t d\mathbf{B}_\tau = \mathbf{B}_t - \mathbf{B}_s \sim \mathcal{N}(\mathbf{0}, (t-s)\mathbf{I})$. It follows that the solution to the hypothesized SDE can be formally expressed as:

$$\mathbf{h}(T) = \int_0^T \mathbf{f}(\mathbf{h}, t) dt + \frac{\sigma}{\sqrt{T}} \int_0^T d\mathbf{B}_t := \mathbf{F}(\mathbf{h}) + \mathbf{B}_T,$$

where $\mathbf{B}_T \sim \mathcal{N}(\mathbf{0}, \sigma^2 \mathbf{I})$ represents additive Gaussian noise and \mathbf{F} denotes deterministic part of the SDE evolution. Proposition B.1 in Appendix B shows that this mechanism obeys (ϵ, δ) -differential privacy whenever $\epsilon < 1$ and $\sigma \geq \sqrt{2 \ln(1.25/\delta)}(S_{\mathbf{F}}/\epsilon)$. The claimed bound on the variance σ follows since the sensitivity $S_{\mathbf{F}}$ is bounded above due to Lipschitz continuity in \mathbf{f} :

$$\begin{aligned} S_{\mathbf{F}} &= \max_{|\mathbf{h}-\mathbf{h}'| \leq 1} |\mathbf{F}(\mathbf{h}) - \mathbf{F}(\mathbf{h}')| \\ &\leq \max_{|\mathbf{h}-\mathbf{h}'| \leq 1} \int_0^T |\mathbf{f}(\mathbf{h}, t) - \mathbf{f}(\mathbf{h}', t)| dt \\ &\leq \max_{|\mathbf{h}-\mathbf{h}'| \leq 1} \int_0^T L_{\mathbf{f}} |\mathbf{h} - \mathbf{h}'| dt \leq TL_{\mathbf{f}}. \quad \square \end{aligned}$$

REMARK 1. Importantly, Theorem 4.1, while stated continuous time, also holds in discrete time—for instance, with the Euler–Maruyama integration method—as long as the function $\mathbf{F}(\mathbf{h}) = \int_0^T \mathbf{f}(\mathbf{h}, t) dt + \epsilon(\mathbf{h})$ appropriately accounts for the quadrature error introduced by this discretization. Assuming Lipschitz continuity in the error term ϵ , the claimed variance bound holds with $TL_{\mathbf{f}}$ replaced by $TL_{\mathbf{f}} + L_{\epsilon} \geq S_{\mathbf{F}}$. While this quadrature error may affect solution accuracy, it does not affect the privacy guarantee, since each Euler sub-step adds a statistically independent fraction of the total required Gaussian noise, and therefore the total amount of noise added is equivalent even if the exact and approximate Gaussian contributions differ. Notably, only the approximate output $\mathbf{h}(T)$ at the final time is private and appropriate for release in this case.

Theorem 4.1 provides an additive noise threshold which guarantees differential privacy in the NSDE forward pass. Although Theorem 4.1 is stated for a constant diffusion term $\mathbf{G}(\mathbf{h}, t) = (\sigma/\sqrt{T})\mathbf{I}$, it continues to hold for a general Lipschitz-continuous, at most linear $\mathbf{G}(\mathbf{h}, t)$, provided the Gaussian random variable $\int_0^T \mathbf{G}(\mathbf{h}, t) dt$

satisfies the stated variance bound for each \mathbf{h} . Moreover, since computing gradients of the NSDE model with respect to its parameters accesses the private input data only through the SDE output $\mathbf{h}(T)$, the following Corollary demonstrating that differential privacy extends to the entire NSDE training process.

COROLLARY 4.2 (NSDE TRAINING IS DIFFERENTIALLY PRIVATE). Consider target privacy parameters $0 < \epsilon' < 1$ and $\delta' > 0$ with a maximum iteration count of K . Then, NSDE training of the drift \mathbf{f} in Theorem 4.1 will be $(\epsilon', K\delta + \delta')$ -differentially private as long as the variance satisfies $\sigma \geq 4\sqrt{K} \ln(1.25/\delta) \ln(1/\delta')(TL/\epsilon')$. Here, $\delta > 0$ is arbitrary and $L = \max_{\mathbf{f}} L_{\mathbf{f}}$ denotes the maximum Lipschitz constant attainable by \mathbf{f} during training.

PROOF. Note that, by the parallel composition principle, mini-batching into disjoint subsets at each iteration does not increase the total privacy leakage, as each individual’s data in the state \mathbf{h} is accessed only once by the SDE mechanism. Similarly, the composition of the NSDE output with a downstream classifier does not degrade (ϵ, δ) -differential privacy guarantees, as these guarantees are immune to post-processing by construction. Consequently, the total privacy leakage in NSDE training is directly proportional to the number of training iterations K , corresponding to the number of accesses to the private input \mathbf{h} . The result follows from the Strong Composition Theorem in Dwork *et al.* [20] [Theorem 3.20, Corollary 3.21], in combination with the variance bound established in Theorem 4.1. \square

REMARK 2. Note that determining the Lipschitz constant L in Corollary 4.2 is most easily accomplished by restricting the NSDE architecture to guarantee a particular Lipschitz bound, see, e.g., [72]. Moreover, it should be noted that the privacy guarantees presented here are not necessarily tight in every case and may be improved with more sophisticated privacy accounting mechanisms, such as those in [1, 15].

Corollary 4.2 guarantees the privacy of NSDE training provided that the diffusion term is constructed to add enough stochastic noise along NSDE solution trajectories. This has the remarkable advantage of privatizing learning without requiring direct intervention in the training process: the network dynamics are already private, therefore no further privacy-preserving modifications are required during the backward pass. In contrast, DP-SGD must use inexact gradient information in order to retain privacy, which can potentially hinder the training process.

5 Empirical Evaluation

We now evaluate the effectiveness of NSDEs, as a DP-learner, in mitigating membership inference attacks. Our evaluation is conducted on the CIFAR-10 and CIFAR-100 datasets. Our NSDE models (**SDENet**) use architectural configurations similar to those of ODENet, consisting of three groups of ODEBlocks with filters with 16, 32, and 64 dimensions, respectively, widened by a factor of 2. In SDENet, stochasticity is introduced by employing an SDE solver within the ODEBlocks, utilizing a stochastic fourth-order Runge-Kutta (RK4) integration method. SDENet also incorporates a hyper-parameter (σ) to control noise intensity, influenced by factors such as time, step size, and the desired level of stochasticity.

²Note that ϵ and δ here are different from those used in Sec 2.3.

Table 2: Contrasting membership inference risks of NSDEs and NODEs. We evaluate both models with five existing attacks.

Model	Method	Acc. (C-10)		Acc. (C-100)		TPR @ 0.1% FPR		TPR @ 1% FPR		AUC		Inference acc.	
		Train	Test	Train	Test	C-10	C-100	C-10	C-100	C-10	C-100	C-10	C-100
NODE (ODENet-16-32-64)	Yeom et al. [79]					0.00%	0.08%	0.00%	1.11%	0.558	0.626	56.59%	61.01%
	Shokri et al. [66]					0.04%	0.06%	0.43%	0.66%	0.448	0.449	50.01%	50.01%
	Song and Mittal [68]	94.3%	84.4%	68.2%	52.4%	0.00%	0.13%	0.00%	1.43%	0.529	0.498	54.22%	51.37%
	Watson et al. [73]					0.00%	0.08%	0.00%	1.11%	0.558	0.626	56.69%	61.01%
	Carlini et al. [5]					1.01%	1.10%	4.22%	5.33%	0.616	0.676	57.65%	62.52%
NSDE (SDENet $k=2$)	Yeom et al. [79]					0.02%	0.05%	0.92%	1.09%	0.525	0.588	52.44%	56.96%
	Shokri et al. [66]					0.09%	0.08%	0.86%	0.85%	0.484	0.473	50.04%	50.00%
	Song and Mittal [68]	81.9%	81.9%	56.5%	50.6%	0.00%	0.12%	0.20%	1.34%	0.509	0.498	50.95%	50.84%
	Watson et al. [73]					0.02%	0.05%	0.91%	1.09%	0.525	0.588	52.44%	56.79%
	Carlini et al. [5]					0.14%	0.43%	1.24%	3.00%	0.525	0.612	51.89%	57.64%

5.1 Effectiveness of NSDEs

Methodology. Here we conduct three comparisons: (1) We compare NSDEs with ResNet-14 to assess whether stochasticity reduces the empirical membership risks. (2) We compare NSDEs with empirical defenses discussed in Sec 2, which lack provable privacy guarantees. (3) We compare NSDEs with “private” ResNet-14 trained with DP-SGD. In (2), we consider four defenses studied in prior work [38, 41, 50, 62]: ℓ^1/ℓ^2 -regularization, MMD-Mixup, and MemGuard. For ℓ^1/ℓ^2 -regularization, we set the penalty parameter λ to 10^{-5} . We use the most robust version of MemGuard as described in Choquette *et al.* [13], which allows for arbitrary adjustments to the confidence vector while preserving the model’s predicted label. For MMD-Mixup, we adopt the implementation from the study by Li *et al.* [50], and set the penalty parameter λ to 5×10^{-4} . When training with DP-SGD, we set the privacy budget ϵ to 8, a common choice for CIFAR-10/-100 in prior work [62]. Note that we use the popular Opacus library³ to implement privacy accounting in NSDE training and to compute the total privacy leakage (ϵ).

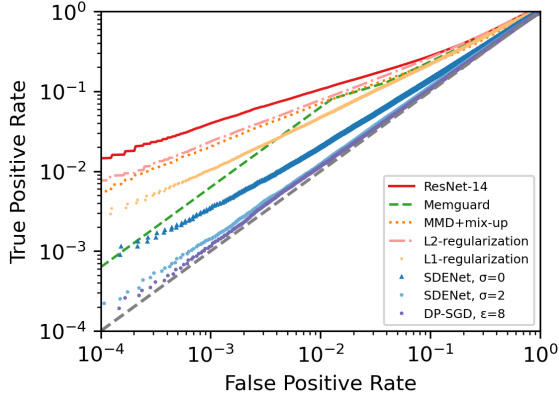


Figure 3: Comparing the effectiveness of different defenses, in CIFAR-10. We use LiRA to assess their membership risks. All defenses, except for SDENets, are applied to ResNet-14.

Defense effectiveness. Figure 3 summarizes our results against LiRA, the strongest-known membership inference attack by Carlini *et al.* [5]. Overall, we first demonstrate that NSDEs effectively

mitigate membership risks. Compared to ResNet-14, a feedforward model that achieves 3.96–10.59% TPR at both 0.1% and 1% FPR, NSDEs with $\sigma=2$ demonstrate approximately two orders of magnitude lower TPRs (0.14–1.24%). We also find that, compared to existing defenses, NSDEs are significantly more effective in reducing membership risks. Compared to the four empirical defenses— ℓ^1/ℓ^2 -regularization, MMD-Mixup and MemGuard—NSDEs with $\sigma=2$ achieves 2–8 \times lower TPR at both 0.1% and 1% FPR. Notably, NSDEs achieve effectiveness comparable to ResNet-14 trained with DP-SGD ($\epsilon=8$). Moreover, it is interesting to observe that NSDEs with $\sigma=0$, the non-private variant of NSDEs, show lower TPRs compared to defended models.

NSDEs with $\sigma=0$ achieve a test accuracy of 83.9%, which, although lower than ResNet-14 at 86.0%, significantly narrows the generalization gap from 12.2% to 5.2%. This reduction results in a markedly lower TPR at 0.1% FPR of 0.4%, compared to 4.0% for ResNet-14. NSDEs with $\sigma=2$ attain a test accuracy of 81.9% and virtually eliminate the generalization gap (-0.02%), further lowering the TPR at 0.1% FPR to 0.1%. When compared to ℓ^1 and ℓ^2 -regularization, NSDEs with $\sigma=2$ not only provide a modest reduction in test accuracy by 4.6%–4.7%, but also enhance defenses, achieving a TPR at 0.1% FPR of 0.14% versus 1.1% for ℓ^1 and 2.4% for ℓ^2). While DP-SGD with $\epsilon=8$ realizes a smallest generalization gap, it incurs significant sacrifices in test accuracy, ranging from 7.5% and 9.5% when compared to NSDEs ($\sigma=0$ and $\sigma=2$) Consequently, NSDEs demonstrates an improved overall performance in terms of both model training (higher test accuracy) and defense against membership inference attacks, making it a more balanced and practical approach. Please refer to Appendix C for more details.

To conduct an in-depth analysis, we present the membership risks of NSDEs and NODEs against five existing attacks in Table 2. The attack success, measured across four metrics, is 4–10 \times lower in NSDEs compared to NODEs. Particularly against LiRA, NSDEs show a TPR of 0.14–1.24% at both 0.1% and 1% FPRs, whereas 1.0–4.22% TPR at the same FPRs in NODEs. To understand where the resilience of NSDEs against these attacks comes, we compare the generalization gap. In NODEs, the gap is 9.9–15.8% points for CIFAR-10 and CIFAR-100, while in NSDEs, it is 0.0–5.9% points. This result implies that *the reduction in membership risks in NSDEs is partly due to a significant reduction in overfitting.*

³Opacus: <https://github.com/pytorch/opacus/>

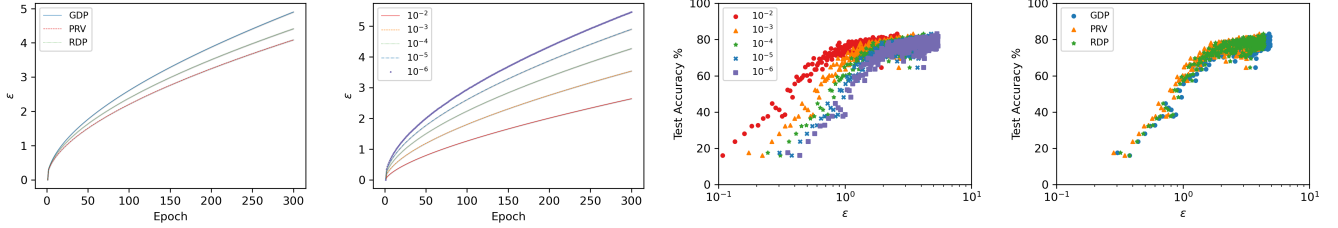


Figure 4: Impact of privacy hyper-parameters on NSDE training in CIFAR-10. We analyze the total privacy leakage (ϵ) in the left two plots and the privacy-utility tradeoff in the right two plots, while varying key hyper-parameters.

5.2 In-depth Analysis of Privacy of NSDEs

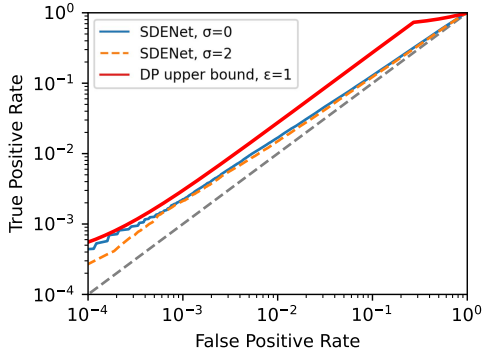


Figure 5: Comparing the empirical membership risks of NSDEs with the theoretical bound by DP-SGD. We use LiRA to measure the membership risks and the theoretical bound when $\epsilon = 1$ is computed by the method presented in [5]. NSDE with $\sigma = 2$ is used to compare, and that with $\sigma = 0$ is its non-private version. The shaded areas give the 68% (darker) and 95% (lighter) confidence intervals.

We next analyze the privacy guarantee (ϵ) provided by NSDEs. Because we theoretically show that NSDEs are DP-learners (with the privacy guarantee equivalent to those of DP-SGD), it is important to understand empirically whether their privacy interactions behave similarly to observations from prior work [35]. We first compare the privacy leakage of NSDEs with the worst-case leakage bound established by DP-SGD. We also examine the impact of privacy hyper-parameters—such as δ and the choice of privacy accounting algorithms—on the guarantee ϵ and the model utility.

Comparison to the theoretical DP-SGD bound. Figure 5 compares the upper-bound of DP-SGD (when $\epsilon = 1$) with the LiRA success on NSDEs with $\sigma = 2$. Note that training NSDEs with $\sigma = 2$ while targeting $\epsilon = 1$ completely destroys the model utility, making any meaningful LiRA success unattainable. We therefore target $\epsilon = 8$ for NSDEs with $\sigma = 2$. This does not compromise the generality of our results, because even against NSDEs with weaker privacy guarantees, the empirical attack (LiRA) does not exceed the DP-SGD bound. We first observe that the attack success of LiRA on NSDEs with $\sigma = 2$ remains within the worst-case leakage bound established by DP-SGD. However, when the diffusion mechanism is absent ($\sigma = 0$), the attack success often goes beyond the DP-SGD bound,

particularly in lower FPR regions (e.g., at 0.1–1% FPR), indicating that privacy is not guaranteed.

We also investigate the impact of privacy hyper-parameters on the guarantee (ϵ) and the privacy-utility tradeoff.

Privacy leakage ϵ over training. The left two figures in Figure 4 illustrate the total privacy leakage ϵ over training. Both figures show that privacy leakage increases with training epochs, as expected, but the growth rate decreases over time. This aligns with empirical findings from prior work on training models with DP-SGD [1].

The leftmost figure presents the privacy leakage computed using three different privacy accountants: Gaussian Differential Privacy (GDP), Renyi Differential Privacy (RDP), and Privacy loss Random Variables (PRVs). GDP accountants consistently yield higher estimates of privacy leakage compared to the other two methods. This is partly because GDP relies on Gaussian approximations, which often deviate from the true privacy loss distribution. In contrast, precise accounting methods like RDP or PRVs, which enable tracking the exact or near-exact cumulative privacy loss, provide tighter privacy bounds. Due to their cumulative nature, we also observe that the differences among the three accountants progressively widens as the number of training epochs increases.

The figure second from the left shows the privacy leakage computed by the GDP accountant across various δ values, ranging from 1×10^{-2} to 1×10^{-6} . Our observations align with the literature: as δ increases, the total privacy leakage (ϵ) also increases. This is because δ represents the probability of catastrophic events where the mechanism may fail to provide privacy guarantees, such as a database breach caused by physical attacks. A larger δ necessitates a relaxation of the privacy requirement, effectively allowing for a slightly higher probability of privacy violations.

Privacy-utility trade-off. The right two figures in Figure 4 illustrate the test accuracy of NSDEs trained with different privacy budgets (ϵ). We record the test accuracy and privacy leakage at each training epoch for the 16 models used in our evaluation, and we plot them. The second figure from the right shows the trade-offs across different failure probabilities (δ). As δ increases, the test accuracy of NSDEs increases under the same privacy budget. This is because a larger δ permits a higher likelihood of privacy leakage. Surprisingly, NSDEs achieve a test accuracy of 80% with $\epsilon = 2$ and $\delta = 10^{-5}$ under GDP, which demonstrates their ability to maintain high utility even at relatively low privacy budgets. The rightmost figure demonstrates that all three accountants produce similar estimates of privacy leakage and test accuracy. However it is important to note the variability in test accuracy: even under the

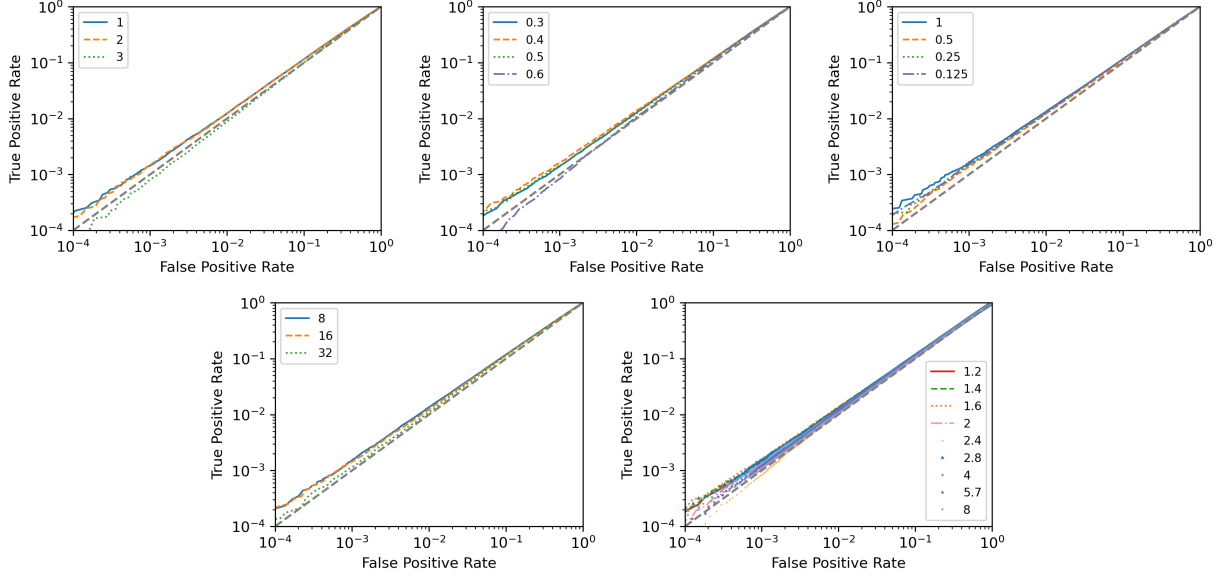


Figure 6: Membership risks of NSDEs trained with different configurations. (Top row, left to right) We illustrate the impact of the number of blocks (n), the level of stochasticity (k), and the step-size (s). (Bottom row, left to right) We show the impact of the integration time T and the noise intensity σ . We use LiRA to assess the membership risks. The results are in CIFAR-10.

same privacy budget, e.g., $\epsilon=2$, test accuracy ranges from 65–82%. We attribute this variance to the factors like randomness introduced by the diffusion term or the training data stochasticity. This suggests that in practice, to train NSDEs with high utility we may need to train the same model multiple times, as shown in prior work [62].

5.3 Impact of NSDE Configurations

We now turn our attention to the impact of NSDE configurations on their membership risks. In this analysis, we maintain consistent hyper-parameters that affect privacy accounting when varying, such as the number of training iterations, batch-size and learning rate. The only exception is the noise intensity (σ) which directly influences the total privacy leakage. We examine five configurations: the number of NSDE blocks n , the level of stochasticity k , the integration time interval T , the step-size $1/s$, and the noise intensity σ . It is important to note that the noise intensity depends on the first three variables, following the formulation $\frac{k}{\sqrt{T/s}}$.

The number of SDE blocks (n). We investigate the impact of adding more SDE blocks on privacy. Due to the post-processing property of DP, connecting multiple SDE blocks sequentially—each with the privacy guarantee ϵ —still results in an overall privacy leakage bounded by ϵ . However, we expect that the diffusion terms in these blocks will introduce random noise multiple times, leading to a substantial decrease in model utility. We vary $n \in \{1, 2, 3\}$.

The top-left panel in Figure 6 illustrates our results. Membership risks associated with NSDE models are consistent when $n=1$ or $n=2$. But employing three SDE blocks reduces the risks by a factor of 2, as measured by TPRs at 0.1–1% FPR. We attribute this reduction to poor generalization when $n=3$. For instance, in CIFAR-10, while NSDEs with $n \in \{1, 2\}$ achieve test accuracy of 81.9–82.4%, models with $n=3$ show significantly lower test accuracy of 74.6%.

Interestingly, unlike NODEs, augmenting the number of SDE blocks in NSDEs leads to a corresponding reduction in membership risks.

The level of stochasticity (k) directly increases the novel intensity (σ) for the Gaussian diffusion term, following the formula $\sigma = \frac{k}{\sqrt{T/s}}$. Increasing k adds more noise to the modeling dynamics, and therefore, a reduction in membership risks. We vary k across $\{0.3, 0.4, 0.5, 0.6\}$, with a default value of 0.5 for all our experiments.

The top-middle panel in Figure 6 illustrates our findings. We show that NSDEs with varying k values effectively mitigate membership risks, as measured by LiRA. With k values up to 0.5, NSDEs exhibit the same level of effectiveness. But when k reaches to 0.6, it completely mitigates the membership risks, bringing the ROC curve below that of a random classifier (a diagonal line). We also examine how each choice of k affects model performance. Increasing the level of stochasticity results in a decrease in model utility. On CIFAR-10, the test accuracy drops from 82.6% to 57.1% as k increases from 0.3 to 0.6. This result implies that the state-of-the-art attack (LiRA) is yet weak so that one can completely mitigate with k that does not significantly degrade model utility.

The integration time interval T . We evaluate the impact of varying integration time intervals by adjusting T and measuring its impact on membership risks. We set T across $\{0.125, 0.25, 0.5, 1\}$, with the default value of $T=1$ used in all our experiments.

The top-right panel in Figure 6 illustrates our findings. Overall, we find no significant interaction between the integration time interval (T) and membership risks. All NSDE models consistently show low membership risks. But theoretically, decreasing T will increase the noise intensity (σ), leading to a smaller privacy leakage (ϵ) with reduced model utility and membership risks.

The step-size ($1/s$), which controls the granularity at which the integration over time T is computed. The increase in s results in a

model less capable of learning details of dynamics in the training data. We vary s across $\{8, 16, 32\}$, with the default value of 16.

The bottom-left panel in Figure 6 summarizes our findings. Overall, we observe only marginal variations in membership risks caused by changes in step size ($1/s$). On CIFAR-10, the membership risks observed at $s = 8$ or 16 are comparable. However, we find a reduction of the risks with $s = 32$, likely because the model lacks learning detailed dynamics from the training data. Our analysis indicates that this reduction comes at the cost of accuracy. A step size of 32 limits NSDEs effectiveness in modeling underlying dynamics, and in consequence, they experience substantial performance degradation. NSDEs at this step size achieve an average accuracy of 35.9%, which is 46.5–46.1% lower than that achieved with s of 8 or 16.

The noise intensity (σ). We finally examine how the noise intensity σ affect membership risks, though this parameter being influenced by our choice of σ , T and s . To evaluate this, we collect results across all combinations of these three configurations from our previous experiments. This results in unique σ values of $\{1.2, 1.4, 1.6, 2.0, 2.8, 4.0, 5.7, 8.0\}$, with duplicates removed. We use LiRA to quantify (empirical) membership risks.

The bottom-right panel in Figure 6 illustrates our results. Overall, we observe that all the noise intensity values we examine effectively mitigate membership risks, consistent with prior work [5], which shows that even the strongest membership inference attacks can be easily countered by a weak privacy guarantee provided by DP-SGD. We also demonstrate that as the noise intensity gets stronger, NSDE’s effectiveness increases. However, it is important how we configure the noise intensity. For instance, setting a lower noise intensity, such as 1.6, by employing a larger step-size (e.g., 32), may appear to reduce membership risks in the figure. But this reduction is primarily due to a substantial drop in model utility, as shown in our analysis of different step-sizes.

5.4 NSDE as a Drop-in Replacement Module

All our evaluations so far assume that a defender trains NSDE models from scratch. This approach often requires more computational resources than expected, and could potentially face pushback, especially when well-performing pre-trained models are available. To address this issue, we present an efficient *replace-then-finetune* strategy. Instead of training NSDEs from scratch, we propose *replacing* the last few layers of an existing pre-trained model with an NSDE block and *then finetune*. This approach reduces computational demands by re-using the majority of pre-trained parameters, as it requires fewer training iterations, while also benefiting from NSDEs’ privacy advantages (based on DP’s composition theorem). It also potentially improves model utility, as fine-tuning leverages the features (i.e., the latent representations/activations obtained at the penultimate layer), a strategy demonstrated to be effective in prior work on training models with DP-SGD [70].

Impact on privacy. Figure 7 demonstrates the effectiveness of the replace-then-finetune strategy. When the last group of the final residual block is replaced with an NSDE block, membership risks are reduced by more than an order of magnitude, particularly in low FPR regions, compared to ResNet-14. However, when compared to the NSDE models trained from scratch, membership risks are higher. This does not imply a difference in the privacy guarantees

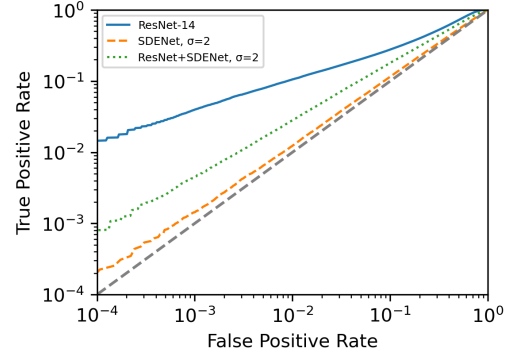


Figure 7: Effectiveness of *replace-and-finetune* strategy. We replace the last residual block of ResNet14 with a NSDE block and then finetune the adapted model on CIFAR-10.

(ϵ) between the two models. Their guarantees remain the same due to the post-processing property.⁴ It is likely that LiRA hits the worst-case privacy leakage against the replace-then-finetuned models, as indicated by the bound shown in Figure 5.

Impact on model utility. We also note that the test accuracy of the replace-then-finetuned models is 84.0%, slightly decreased from 86.0% of ResNet-14. But the reduction is comparatively smaller than that we observe in NSDEs trained from scratch, which achieves a test accuracy of 81.9%. We also note that this approach potentially reduces the computational demands of NSDE training. Notably, we observe that test accuracy stabilizes after 150 epochs, which is half the total number of epochs we use for training NSDEs. As shown in our theoretical analysis in Sec 4.1, a reduction in the number of training iterations (K) also decreases the total privacy leakage of the trained models. Our results demonstrate the effectiveness of the replace-then-finetune strategy in reducing membership risks while achieving improved utility and lowering computational demands.

6 Related Work

Privacy attacks on machine learning. Membership inference attacks, due to its simplest formulation—where an adversary knows a particular instance and then only aims to infer its membership, represent the worst-case privacy leakage and have been widely studied as a privacy auditing mechanism. But there have been other types of privacy attacks studied in machine learning.

Fredrikson et al. [23] introduced the concept of *model inversion*, which are reconstruction attacks designed to reverse-engineer training samples or reconstructing sensitive information in the training data not exposed to public. Initial work [23] focused on attacks targeting simple linear models, while subsequent work [22, 77] focuses on non-linear models such as decision trees and/or neural networks. In particular, against neural networks, adversaries iteratively update instances by computing gradients, gradually refining them until they resemble the original training data.

If a model inversion adversary focuses on inferring the value of unknown sensitive attributes, such as gender or race, of particular training records, it is referred to as *attribute inference attacks* [79]. A typical adversary exploits the query access to the target model

⁴Note that the last NSDE block is randomly initialized and fine-tuned.

to learn sensitive attributes in the (partial) training data. Diverse attack methodologies [23, 55, 79] have been proposed, and attribute inference has been exploited across different domains, such as social media [9, 25–27, 39, 83] or recommendation systems [74, 76].

The recent emergence of advanced neural networks, such as language models, diffusion models, and differential equation-based neural networks like NODEs, necessitates the adaptation and evaluation of existing privacy attacks on these models. The most active area of study focuses on language models and diffusion models. Prior work [6–8] extended these privacy attacks to these models and demonstrated their vulnerability to membership inference attacks or model inversion, also referred to as data extraction attacks.

No prior work has yet studied the vulnerability of emerging differential equation-based neural networks, such as NODEs and NSDEs, to privacy attacks. Our work addresses this knowledge gap by presenting the first study on understanding and mitigating the membership risks associated with NODEs.

Security and privacy of NODEs and NSDEs. In the literature, security and privacy aspects of NODEs and NSDEs have mainly focused on countering *adversarial examples* [28] and learning stable, robust dynamics. Time-invariant steady neural ODEs (TisODEs) [31] empirically demonstrated that NODEs are more resilient to random Gaussian noise and to adversarial examples than traditional convolutional neural networks. TisODEs proposed a steady-state regularizer that minimizes the deviation of the hidden states $\mathbf{h}(t)$ after a terminal time, T (i.e., steady-state after T), leading to a stable dynamics. In [40], a method to guide trajectories toward Lyapunov-stable equilibrium points, resulting in NODEs extracting hidden features around these stable points. This work empirically shows that the stability leads to improved robustness against adversarial examples. The same approach has been further extended to a non-autonomous dynamics systems, where trajectories are guided to asymptotically stable equilibrium point [52]. In [81], the investigation on the robustness has been extended to high-dimensional NODEs, presenting graph-based tools for robustness verification.

Other techniques to enhance NODEs robustness include skew-symmetric ODE blocks [33] and integrating Gaussian process [2] both providing empirical improvements in robustness. While not explicitly robustness-focused, some efforts contribute similarly—regularizing NODE dynamics. Kinetic and Jacobian regularizers [21] and high-order derivatives regularizers [42] have been introduced and shown effective in regularizing the dynamics to be smooth. A method proposed in STEER [24] mitigate the learning of stiff ODEs by randomizing terminal times during training.

There are only handful of papers that have investigated security and privacy aspects of NSDEs. Some of those work include [37], which showed that the attributions computed over NSDEs are less noisy, visually sharper, and quantitatively more robust than those computed on the deterministic NODEs. Liu et al. [54] demonstrated that NSDEs improve robustness against adversarial examples. In general context, NSDEs have been widely adopted as a tool to estimate uncertainty [44, 46], as a part of generative models [43], and physics simulation with probabilistic state transitions [3].

7 Conclusion

Our work studies the privacy implications of emerging neural networks, NODEs, using membership inference attacks as a vehicle. We are the first work that presents a *comprehensive analysis* of their membership risks. Our major findings are: (1) NODEs are twice as resilient to existing membership inference attacks compared to conventional feedforward models like ResNets, while achieving comparable accuracy. (2) This privacy benefit is not due to reduced model overfitting. NODEs exhibit a high generalization gap, and we attribute this benefit to their approach of modeling data as a system of ODEs. (3) In addition to that, we show that advanced, non-stochastic variants of NODEs offer reduced overfitting, resulting in an improved accuracy with a reduction in membership risks.

Our analysis does *not* imply that NODEs are free from membership risks. We study an approach to further reduce the risks: NSDEs, a stochastic adaptation of NODEs that incorporates an additional diffusion term in system modeling. Most importantly, we *formally show* that the diffusion term works as a differentially-private (DP) mechanism, thereby making NSDEs as DP-learners. Our theoretical analysis shows that the privacy guarantee (ϵ) offered by NSDEs is equivalent to that of DP-SGD when using identical mini-batch training configurations. We demonstrate empirically that NSDEs are more effective at reducing membership risks compared to existing defenses with no privacy guarantee. Unlike DP-SGD, they achieve this mitigation with a smaller impact on model utility.

Moreover, we present an effective strategy, *replace-then-finetune*, for using NSDEs as a drop-in replacement module to enhance privacy. We replace the last few layers of a pre-trained conventional feedforward model with an NSDE block and finetune the adapted model for a few epochs. We demonstrate that this strategy reduces the membership risks of the original pre-trained model by an order of magnitude, while achieving model utility greater than that of DP-SGD, with only half the computational costs for training.

Our work demonstrates that systems learned by neural networks can be effectively *modeled with privacy*. Our results imply that advanced neural networks employing diffusion mechanisms, such as stable diffusion models, may, with careful modeling, operate as inherently private models while delivering enhanced performance. As future work, investigating this private system may offer valuable insights into how DP influences what neural networks learn. We also hope that our work inspires the adoption of the replace-then-finetune strategy as an effective approach to enhancing privacy.

Acknowledgements

S.H. is partially supported by the Google Faculty Research Award (2023). K.L. acknowledges support from the U.S. National Science Foundation under grant IIS 2338909. A.G. acknowledges support from the U.S. Department of Energy, Office of Advanced Scientific Computing Research under the Scalable, Efficient, and Accelerated Causal Reasoning for Earth and Embedded Systems (SEA-CROGS) project. Sandia National Laboratories is a multimission laboratory managed and operated by National Technology & Engineering Solutions of Sandia, LLC, a wholly owned subsidiary of Honeywell International Inc., for the U.S. Department of Energy's National Nuclear Security Administration under contract DE-NA0003525. This paper describes objective technical results and analysis. Any

subjective views or opinions that might be expressed in the paper do not necessarily represent the views of the U.S. Department of Energy or the United States Government. This article has been co-authored by an employee of National Technology & Engineering Solutions of Sandia, LLC under Contract No. DE-NA0003525 with the U.S. Department of Energy (DOE). The employee owns all right, title and interest in and to the article and is solely responsible for its contents. The United States Government retains and the publisher, by accepting the article for publication, acknowledges that the United States Government retains a non-exclusive, paid-up, irrevocable, world-wide license to publish or reproduce the published form of this article or allow others to do so, for United States Government purposes. The DOE will provide public access to these results of federally sponsored research in accordance with the DOE Public Access Plan <https://www.energy.gov/downloads/doe-public-access-plan>.

References

- [1] Martin Abadi, Andy Chu, Ian Goodfellow, H. Brendan McMahan, Ilya Mironov, Kunal Talwar, and Li Zhang. 2016. Deep Learning with Differential Privacy. In *Proceedings of the 2016 ACM SIGSAC Conference on Computer and Communications Security (Vienna, Austria) (CCS '16)*. Association for Computing Machinery, New York, NY, USA, 308–318. doi:10.1145/2976749.2978318
- [2] Srinivas Anumasa and PK Srijith. 2021. Improving robustness and uncertainty modelling in neural ordinary differential equations. In *Proceedings of the IEEE/CVF Winter Conference on Applications of Computer Vision*. 4053–4061.
- [3] Anudhyan Boral, Zhong Yi Wan, Leonardo Zepeda-Núñez, James Lottes, Qing Wang, Yi-fan Chen, John Anderson, and Fei Sha. 2024. Neural ideal large eddy simulation: Modeling turbulence with neural stochastic differential equations. *Advances in Neural Information Processing Systems* 36 (2024).
- [4] John Charles Butcher. 2016. *Numerical Methods for Ordinary Differential Equations*. John Wiley & Sons.
- [5] Nicholas Carlini, Steve Chien, Milad Nasr, Shuang Song, Andreas Terzis, and Florian Tramèr. 2022. Membership Inference Attacks From First Principles. In *2022 IEEE Symposium on Security and Privacy (SP)*. 1897–1914. doi:10.1109/SP46214.2022.9833649
- [6] Nicolas Carlini, Jamie Hayes, Milad Nasr, Matthew Jagielski, Vikash Sehwal, Florian Tramèr, Borja Balle, Daphne Ippolito, and Eric Wallace. 2023. Extracting Training Data from Diffusion Models. In *32nd USENIX Security Symposium (USENIX Security 23)*. USENIX Association, Anaheim, CA, 5253–5270. <https://www.usenix.org/conference/usenixsecurity23/presentation/carlini>
- [7] Nicholas Carlini, Chang Liu, Úlfar Erlingsson, Jernej Kos, and Dawn Song. 2019. The Secret Sharer: Evaluating and Testing Unintended Memorization in Neural Networks. In *28th USENIX Security Symposium (USENIX Security 19)*. USENIX Association, Santa Clara, CA, 267–284. <https://www.usenix.org/conference/usenixsecurity19/presentation/carlini>
- [8] Nicholas Carlini, Florian Tramèr, Eric Wallace, Matthew Jagielski, Ariel Herbert-Voss, Katherine Lee, Adam Roberts, Tom Brown, Dawn Song, Úlfar Erlingsson, Alina Oprea, and Colin Raffel. 2021. Extracting Training Data from Large Language Models. In *30th USENIX Security Symposium (USENIX Security 21)*. USENIX Association, 2633–2650. <https://www.usenix.org/conference/usenixsecurity21/presentation/carlini-extracting>
- [9] Abdelber Chaabane, Gergely Acs, Mohamed Ali Kaafar, et al. 2012. You are what you like! information leakage through users' interests. In *Proceedings of the 19th annual network & distributed system security symposium (NDSS)*. Citeseer.
- [10] Ricky T. Q. Chen, Yulia Rubanova, Jesse Bettencourt, and David K Duvenaud. 2018. Neural Ordinary Differential Equations. In *Advances in Neural Information Processing Systems*, S. Bengio, H. Wallach, H. Larochelle, K. Grauman, N. Cesa-Bianchi, and R. Garnett (Eds.), Vol. 31. Curran Associates, Inc. https://proceedings.neurips.cc/paper_files/paper/2018/file/69386f6bb1dfed68692a24c8686939b9-Paper.pdf
- [11] Suneghyeon Cho, Sanghyun Hong, Kookjin Lee, and Noseong Park. 2022. AdamNODEs: When Neural ODE Meets Adaptive Moment Estimation. arXiv:2207.06066 [cs.LG] <https://arxiv.org/abs/2207.06066>
- [12] Woojin Cho, Seunghyeon Cho, Hyundong Jin, Jinsung Jeon, Kookjin Lee, Sanghyun Hong, Dongeun Lee, Jonghyun Choi, and Noseong Park. 2024. Operator-Learning-Inspired Modeling of Neural Ordinary Differential Equations. In *Proceedings of the AAAI Conference on Artificial Intelligence*, Vol. 38. 11543–11551.
- [13] Christopher A Choquette-Choo, Florian Tramèr, Nicholas Carlini, and Nicolas Papernot. 2021. Label-only membership inference attacks. In *International conference on machine learning*. PMLR, 1964–1974.
- [14] Edward De Brouwer, Jaak Simm, Adam Arany, and Yves Moreau. 2019. GRU-ODE-Bayes: Continuous modeling of sporadically-observed time series. *Advances in neural information processing systems* 32 (2019).
- [15] Jinshuo Dong, Aaron Roth, and Weijie J Su. 2022. Gaussian differential privacy. *Journal of the Royal Statistical Society: Series B (Statistical Methodology)* 84, 1 (2022), 3–37.
- [16] John R Dormand and Peter J Prince. 1980. A family of embedded Runge–Kutta formulae. *Journal of computational and applied mathematics* 6, 1 (1980), 19–26.
- [17] Emilien Dupont, Arnaud Doucet, and Yee Whye Teh. 2019. Augmented Neural ODEs. In *Advances in Neural Information Processing Systems*, H. Wallach, H. Larochelle, A. Beygelzimer, F. d'Alché-Buc, E. Fox, and R. Garnett (Eds.), Vol. 32. Curran Associates, Inc. https://proceedings.neurips.cc/paper_files/paper/2019/file/21be9a4bd4f81549a9d1d241981cec3c-Paper.pdf
- [18] Emilien Dupont, Arnaud Doucet, and Yee Whye Teh. 2019. Augmented neural odes. *Advances in Neural Information Processing Systems* 32 (2019).
- [19] Cynthia Dwork. 2006. Differential privacy. In *International colloquium on automata, languages, and programming*. Springer, 1–12.
- [20] Cynthia Dwork and Aaron Roth. 2014. The Algorithmic Foundations of Differential Privacy. *Foundations and Trends in Theoretical Computer Science* 9, 3–4 (2014), 211–407.
- [21] Chris Finlay, Jörn-Henrik Jacobsen, Levon Nurbekyan, and Adam Oberman. 2020. How to train your neural ODE: The world of Jacobian and kinetic regularization. In *International conference on machine learning*. PMLR, 3154–3164.
- [22] Matt Fredrikson, Somesh Jha, and Thomas Ristenpart. 2015. Model Inversion Attacks that Exploit Confidence Information and Basic Countermeasures. In *Proceedings of the 22nd ACM SIGSAC Conference on Computer and Communications Security (Denver, Colorado, USA) (CCS '15)*. Association for Computing Machinery, New York, NY, USA, 1322–1333. doi:10.1145/2810103.2813677
- [23] Matthew Fredrikson, Eric Lantz, Somesh Jha, Simon Lin, David Page, and Thomas Ristenpart. 2014. Privacy in Pharmacogenetics: An End-to-End Case Study of Personalized Warfarin Dosing. In *USENIX Security Symposium*.
- [24] Arnab Ghosh, Harkirat Behl, Emilien Dupont, Philip Torr, and Vinay Namboodiri. 2020. Steer: Simple temporal regularization for neural ODE. *Advances in Neural Information Processing Systems* 33 (2020), 14831–14843.
- [25] Neil Zhenqiang Gong and Bin Liu. 2016. You Are Who You Know and How You Behave: Attribute Inference Attacks via Users' Social Friends and Behaviors. In *25th USENIX Security Symposium (USENIX Security 16)*. USENIX Association, Austin, TX, 979–995. <https://www.usenix.org/conference/usenixsecurity16/technical-sessions/presentation/gong>
- [26] Neil Zhenqiang Gong and Bin Liu. 2018. Attribute Inference Attacks in Online Social Networks. *ACM Trans. Priv. Secur.* 21, 1, Article 3 (Jan. 2018), 30 pages. doi:10.1145/3154793
- [27] Neil Zhenqiang Gong, Ameet Talwalkar, Lester Mackey, Ling Huang, Eui Chul Richard Shin, Emil Stefanov, Elaine (Runting) Shi, and Dawn Song. 2014. Joint Link Prediction and Attribute Inference Using a Social-Attribute Network. *ACM Trans. Intell. Syst. Technol.* 5, 2, Article 27 (April 2014), 20 pages. doi:10.1145/2594455
- [28] Ian Goodfellow, Jonathon Shlens, and Christian Szegedy. 2015. Explaining and Harnessing Adversarial Examples. In *International Conference on Learning Representations*. <http://arxiv.org/abs/1412.6572>
- [29] Samuel Gretydanus, Misko Dzamba, and Jason Yosinski. 2019. Hamiltonian neural networks. *Advances in neural information processing systems* 32 (2019).
- [30] Anthony Gruber, Kookjin Lee, and Nathaniel Trask. 2024. Reversible and irreversible bracket-based dynamics for deep graph neural networks. *Advances in Neural Information Processing Systems* 36 (2024).
- [31] YAN Hanshu, DU Jiawei, TAN Vincent, and FENG Jiashi. 2020. On Robustness of Neural Ordinary Differential Equations. In *International Conference on Learning Representations*.
- [32] Kaiming He, Xiangyu Zhang, Shaoqing Ren, and Jian Sun. 2016. Deep residual learning for image recognition. In *Proceedings of the IEEE conference on computer vision and pattern recognition*. 770–778.
- [33] Yifei Huang, Yaodong Yu, Hongyang Zhang, Yi Ma, and Yuan Yao. 2022. Adversarial robustness of stabilized neural ODE might be from obfuscated gradients. In *Mathematical and Scientific Machine Learning*. PMLR, 497–515.
- [34] Kazuki Irie, Francesco Faccio, and Jürgen Schmidhuber. 2022. Neural differential equations for learning to program neural nets through continuous learning rules. *Advances in Neural Information Processing Systems* 35 (2022), 38614–38628.
- [35] Bargav Jayaraman and David Evans. 2019. Evaluating Differentially Private Machine Learning in Practice. In *28th USENIX Security Symposium (USENIX Security 19)*. USENIX Association, Santa Clara, CA, 1895–1912. <https://www.usenix.org/conference/usenixsecurity19/presentation/jayaraman>
- [36] Jinsung Jeon, JEONGHAK KIM, Haryong Song, Seunghyeon Cho, and Noseong Park. 2022. GT-GAN: General Purpose Time Series Synthesis with Generative Adversarial Networks. In *Advances in Neural Information Processing Systems*, Alice H. Oh, Alekh Agarwal, Danielle Belgrave, and Kyunghyun Cho (Eds.). <https://openreview.net/forum?id=e26VHWvUXeX>
- [37] Sumit Jha, Rickard Ewetz, Alvaro Velasquez, and Susmit Jha. 2021. On smoother attributions using neural stochastic differential equations. In *30th International*

- Joint Conference on Artificial Intelligence (IJCAI), 2021.*
- [38] Jinyuan Jia, Ahmed Salem, Michael Backes, Yang Zhang, and Neil Zhenqiang Gong. 2019. MemGuard: Defending against Black-Box Membership Inference Attacks via Adversarial Examples. In *Proceedings of the 2019 ACM SIGSAC Conference on Computer and Communications Security* (London, United Kingdom) (CCS '19). Association for Computing Machinery, New York, NY, USA, 259–274. doi:10.1145/3319535.3363201
- [39] Jinyuan Jia, Binghui Wang, Le Zhang, and Neil Zhenqiang Gong. 2017. AttrInfer: Inferring User Attributes in Online Social Networks Using Markov Random Fields. In *Proceedings of the 26th International Conference on World Wide Web* (Perth, Australia) (WWW '17). International World Wide Web Conferences Steering Committee, Republic and Canton of Geneva, CHE, 1561–1569. doi:10.1145/3038912.3052695
- [40] Qiyu Kang, Yang Song, Qinxu Ding, and Wee Peng Tay. 2021. Stable neural ODE with Lyapunov-stable equilibrium points for defending against adversarial attacks. *Advances in Neural Information Processing Systems* 34 (2021), 14925–14937.
- [41] Yigitcan Kaya, Sanghyun Hong, and Tudor Dumitras. 2020. On the Effectiveness of Regularization Against Membership Inference Attacks. *CoRR* abs/2006.05336 (2020). arXiv:2006.05336 <https://arxiv.org/abs/2006.05336>
- [42] Jacob Kelly, Jesse Bettencourt, Matthew J Johnson, and David K Duvenaud. 2020. Learning differential equations that are easy to solve. *Advances in Neural Information Processing Systems* 33 (2020), 4370–4380.
- [43] Patrick Kidger, James Foster, Xuechen Li, and Terry J Lyons. 2021. Neural sdes as infinite-dimensional GANs. In *International conference on machine learning*. PMLR, 5453–5463.
- [44] Patrick Kidger, James Foster, Xuechen Chen Li, and Terry Lyons. 2021. Efficient and accurate gradients for neural sdes. *Advances in Neural Information Processing Systems* 34 (2021), 18747–18761.
- [45] Patrick Kidger, James Morrill, James Foster, and Terry Lyons. 2020. Neural Controlled Differential Equations for Irregular Time Series. *Advances in Neural Information Processing Systems* (2020).
- [46] Lingkai Kong, Jimeng Sun, and Chao Zhang. 2020. SDE-Net: Equipping Deep Neural Networks with Uncertainty Estimates. In *International Conference on Machine Learning*. PMLR, 5405–5415.
- [47] Alex Krizhevsky. 2009. *Learning Multiple Layers of Features from Tiny Images*. Technical Report.
- [48] Jaehoon Lee, Chan Kim, Gyumin Lee, Haksoo Lim, Jeongwhan Choi, Kookjin Lee, Dongeun Lee, Sanghyun Hong, and Noseong Park. 2024. HyperNetwork Approximating Future Parameters for Time Series Forecasting under Temporal Drifts. In *NeurIPS 2023 Workshop on Distribution Shifts: New Frontiers with Foundation Models*. <https://openreview.net/forum?id=7yVBYSPI8Z>
- [49] Kookjin Lee, Nathaniel Trask, and Panos Stinis. 2021. Machine learning structure preserving brackets for forecasting irreversible processes. *Advances in Neural Information Processing Systems* 34 (2021), 5696–5707.
- [50] Jiacheng Li, Ninghui Li, and Bruno Ribeiro. 2021. Membership Inference Attacks and Defenses in Classification Models. In *Proceedings of the Eleventh ACM Conference on Data and Application Security and Privacy* (Virtual Event, USA) (CODASPY '21). Association for Computing Machinery, New York, NY, USA, 5–16. doi:10.1145/3422337.3447836
- [51] Xuechen Li, Ting-Kam Leonard Wong, Ricky TQ Chen, and David Duvenaud. 2020. Scalable gradients for stochastic differential equations. In *International Conference on Artificial Intelligence and Statistics*. PMLR, 3870–3882.
- [52] Xiyuan Li, Zou Xin, and Weiwei Liu. 2022. Defending against adversarial attacks via neural dynamic system. *Advances in Neural Information Processing Systems* 35 (2022), 6372–6383.
- [53] Xuanqing Liu, Tesi Xiao, Si Si, Qin Cao, Sanjiv Kumar, and Cho-Jui Hsieh. 2019. Neural SDE: Stabilizing neural ode networks with stochastic noise. *arXiv preprint arXiv:1906.02355* (2019).
- [54] Xuanqing Liu, Tesi Xiao, Si Si, Qin Cao, Sanjiv Kumar, and Cho-Jui Hsieh. 2020. How Does Noise Help Robustness? Explanation and Exploration under the Neural SDE Framework. In *Proceedings of the IEEE/CVF Conference on Computer Vision and Pattern Recognition (CVPR)*.
- [55] Shaguftha Mehnaz, Sayanton V. Dibbo, Ehsanul Kabir, Ninghui Li, and Elisa Bertino. 2022. Are Your Sensitive Attributes Private? Novel Model Inversion Attribute Inference Attacks on Classification Models. In *31st USENIX Security Symposium (USENIX Security 22)*. USENIX Association, Boston, MA, 4579–4596. <https://www.usenix.org/conference/usenixsecurity22/presentation/mehnaz>
- [56] James Morrill, Cristopher Salvi, Patrick Kidger, and James Foster. 2021. Neural rough differential equations for long time series. In *International Conference on Machine Learning*. PMLR, 7829–7838.
- [57] Milad Nasr, Reza Shokri, and Amir Houmansadr. 2019. Comprehensive privacy analysis of deep learning: Passive and active white-box inference attacks against centralized and federated learning. In *2019 IEEE symposium on security and privacy (SP)*. IEEE, 739–753.
- [58] Nghia Nguyen, Tan Minh Nguyen, Võ Thục Khánh Huyen, Stanley Osher, and Thieu Vo. 2022. Improving Neural Ordinary Differential Equations with Nesterov's Accelerated Gradient Method. In *Advances in Neural Information Processing Systems*.
- [59] Alexander Norcliffe, Cristian Bodnar, Ben Day, Nikola Simidjievski, and Pietro Liò. 2020. On second order behaviour in augmented neural odes. *Advances in Neural Information Processing Systems* 33 (2020), 5911–5921.
- [60] Viktor Oganesyan, Alexandra Volokhova, and Dmitry Vetrov. 2020. Stochasticity in neural ODEs: An empirical study. *arXiv preprint arXiv:2002.09779* (2020).
- [61] Eckhard Platen and Nicola Bruti-Liberati. 2010. *Numerical solution of stochastic differential equations with jumps in finance*. Vol. 64. Springer Science & Business Media.
- [62] Natalia Ponomareva, Sergei Vassilvitskii, Zheng Xu, Brendan McMahan, Alexey Kurakin, and Chiyuan Zhang. 2023. How to DP-fy ML: A Practical Tutorial to Machine Learning with Differential Privacy. In *Proceedings of the 29th ACM SIGKDD Conference on Knowledge Discovery and Data Mining* (Long Beach, CA, USA) (KDD '23). Association for Computing Machinery, New York, NY, USA, 5823–5824. doi:10.1145/3580305.3599561
- [63] Lev Semenovich Pontryagin. 2018. *Mathematical Theory of Optimal Processes*. Routledge.
- [64] Christopher Rackauckas, Yingbo Ma, Julius Martensen, Collin Warner, Kirill Zubov, Rohit Supekar, Dominic Skinner, Ali Ramadhan, and Alan Edelman. 2020. Universal differential equations for scientific machine learning. *arXiv preprint arXiv:2001.04385* (2020).
- [65] Yulia Rubanova, Ricky TQ Chen, and David K Duvenaud. 2019. Latent ordinary differential equations for irregularly-sampled time series. *Advances in neural information processing systems* 32 (2019).
- [66] Reza Shokri, Marco Stronati, Congzheng Song, and Vitaly Shmatikov. 2017. Membership Inference Attacks Against Machine Learning Models. In *2017 IEEE Symposium on Security and Privacy (SP)*. 3–18. doi:10.1109/SP.2017.41
- [67] Liwei Song and Prateek Mittal. 2021. Systematic Evaluation of Privacy Risks of Machine Learning Models. In *30th USENIX Security Symposium (USENIX Security 21)*. USENIX Association, 2615–2632. <https://www.usenix.org/conference/usenixsecurity21/presentation/song>
- [68] Yang Song, Jascha Sohl-Dickstein, Diederik P Kingma, Abhishek Kumar, Stefano Ermon, and Ben Poole. 2021. Score-Based Generative Modeling through Stochastic Differential Equations. In *International Conference on Learning Representations*. <https://openreview.net/forum?id=PxTIG12RRHS>
- [69] Steven H Strogatz. 2018. *Nonlinear Dynamics and Chaos: With Applications to Physics, Biology, Chemistry, and Engineering*. CRC press.
- [70] Florian Tramer and Dan Boneh. 2021. Differentially Private Learning Needs Better Features (or Much More Data). In *International Conference on Learning Representations*. <https://openreview.net/forum?id=YTWgvPFOQD>
- [71] Yogesh Verma, Markus Heinonen, and Vikas Garg. 2024. ClimODE: Climate and Weather Forecasting with Physics-informed Neural ODEs. In *The Twelfth International Conference on Learning Representations*.
- [72] Ruigang Wang and Ian Manchester. 2023. Direct parameterization of lipschitz-bounded deep networks. In *International Conference on Machine Learning*. PMLR, 36093–36110.
- [73] Lauren Watson, Chuan Guo, Graham Cormode, and Alexandre Sablayrolles. 2022. On the Importance of Difficulty Calibration in Membership Inference Attacks. In *International Conference on Learning Representations*. <https://openreview.net/forum?id=3elrli0TwQ>
- [74] Udi Weinsberg, Smriti Bhagat, Stratis Ioannidis, and Nina Taft. 2012. BlurMe: inferring and obfuscating user gender based on ratings. In *Proceedings of the Sixth ACM Conference on Recommender Systems* (Dublin, Ireland) (RecSys '12). Association for Computing Machinery, New York, NY, USA, 195–202. doi:10.1145/2365952.2365989
- [75] Fan Wu, Woojin Cho, David Korotky, Sanghyun Hong, Donsub Rim, Noseong Park, and Kookjin Lee. 2024. Identifying Contemporaneous and Lagged Dependence Structures by Promoting Sparsity in Continuous-time Neural Networks. In *Proceedings of the 33rd ACM International Conference on Information and Knowledge Management*. 2534–2543.
- [76] Le Wu, Yonghui Yang, Kun Zhang, Richang Hong, Yanjie Fu, and Meng Wang. 2020. Joint Item Recommendation and Attribute Inference: An Adaptive Graph Convolutional Network Approach. In *Proceedings of the 43rd International ACM SIGIR Conference on Research and Development in Information Retrieval* (Virtual Event, China) (SIGIR '20). Association for Computing Machinery, New York, NY, USA, 679–688. doi:10.1145/3397271.3401144
- [77] Xi Wu, Matthew Fredrikson, Somesh Jha, and Jeffrey F. Naughton. 2016. A Methodology for Formalizing Model-Inversion Attacks. In *2016 IEEE 29th Computer Security Foundations Symposium (CSF)*. 355–370. doi:10.1109/CSF.2016.32
- [78] Hedi Xia, Vai Suliafu, Hangjie Ji, Tan Minh Nguyen, Andrea Bertozzi, Stanley Osher, and Bao Wang. 2021. Heavy Ball Neural Ordinary Differential Equations. In *Advances in Neural Information Processing Systems*. A. Beygelzimer, Y. Dauphin, P. Liang, and J. Wortman Vaughan (Eds.). <https://openreview.net/forum?id=fYlFs9rTmQ>

- [79] Samuel Yeom, Irene Giacomelli, Matt Fredrikson, and Somesh Jha. 2018. Privacy Risk in Machine Learning: Analyzing the Connection to Overfitting. In *2018 IEEE 31st Computer Security Foundations Symposium (CSF)*. 268–282. doi:10.1109/CSF.2018.00027
- [80] Cagatay Yildiz, Markus Heinonen, and Harri Lahdesmaki. 2019. Ode2vae: Deep generative second order odes with bayesian neural networks. *Advances in Neural Information Processing Systems* 32 (2019).
- [81] Mustafa Zeqiri, Mark Niklas Mueller, Marc Fischer, and Martin Vechev. 2023. Efficient Certified Training and Robustness Verification of Neural ODEs. In *The Eleventh International Conference on Learning Representations*.
- [82] Guangsheng Zhang, Bo Liu, Huan Tian, Tianqing Zhu, Ming Ding, and Wanlei Zhou. 2024. How Does a Deep Learning Model Architecture Impact Its Privacy? A Comprehensive Study of Privacy Attacks on {CNNs} and Transformers. In *33rd USENIX Security Symposium (USENIX Security 24)*. 6795–6812.
- [83] Elena Zheleva and Lise Getoor. 2009. To join or not to join: the illusion of privacy in social networks with mixed public and private user profiles. In *Proceedings of the 18th International Conference on World Wide Web (Madrid, Spain) (WWW '09)*. Association for Computing Machinery, New York, NY, USA, 531–540. doi:10.1145/1526709.1526781
- [84] Yaofeng Desmond Zhong, Biswadip Dey, and Amit Chakraborty. 2020. Symplectic ODE-Net: Learning Hamiltonian Dynamics with Control. In *International Conference on Learning Representations*.

A Model Architectures

We adopt architectures examined in prior work [60].

ResNet-14

$$\begin{aligned} &[\text{Conv2d} \rightarrow \text{BN} \rightarrow \text{ResBlock} \times 3 \rightarrow \text{BN} \rightarrow \text{Conv2d} \\ &\quad \rightarrow \text{ResBlock} \times 3 \rightarrow \text{BN} \rightarrow \text{Conv2d} \\ &\quad \rightarrow \text{ResBlock} \times 3 \\ &\quad \rightarrow \text{AdaptiveAvgPool2d} \rightarrow \text{Linear}] \end{aligned},$$

where ResBlock is composed as

$$[\text{BN} \rightarrow \text{Conv2d} \rightarrow \text{BN} \rightarrow \text{Conv2d}].$$

ODENet-16-32-64

$$\begin{aligned} &[\text{Conv2d} \rightarrow \text{BN} \rightarrow \text{ODEBlock} \rightarrow \text{BN} \rightarrow \text{Conv2d} \\ &\quad \rightarrow \text{ODEBlock} \rightarrow \text{BN} \rightarrow \text{Conv2d} \\ &\quad \rightarrow \text{ODEBlock} \\ &\quad \rightarrow \text{AdaptiveAvgPool2d} \rightarrow \text{Linear}] \end{aligned},$$

where ODEBlock is

$$[\text{ConcatConv2d} \rightarrow \text{ConcatConv2d}],$$

ConcatConv2d augments x by concatenating an additional feature channel derived from t .

The ResNet/ODENet model architecture consists of convolutional layers interspersed with batch normalization, integration blocks, downsampling, and fully connected layers.

The integration blocks are implemented as ResBlocks for ResNet and ODEBlocks for ODENet and SDENet. Each ResBlock or ODEBlock processes its inputs through a structured sequence of layers, adapting dynamically to varying input dimensions. Generally, a ResBlock begins with a Batch Normalization (BN) layer that normalizes the inputs, followed by a convolutional (Conv2d) layer. This convolutional (Conv2d) layer is configured to match the input dimension while maintaining the channel size, typically using a kernel size of 3×3 , a stride of 1, and padding of 1 to preserve spatial dimensions. The convolution's output undergoes another normalization via a second BN layer before being passed through an additional convolutional (Conv2d) layer with identical specifications to preserve feature depth and spatial integrity. Conversely, each ODEBlock incorporates time dynamics into the feature processing. It utilizes ConcatConv2d layers, which extend the input features by integrating a time channel, thus increasing the input channels by one. The first ConcatConv2d layer, therefore, takes in one additional channel compared to the feature channels—modifying the input dimension based on the incoming feature map size. This layer outputs feature maps that maintain the original dimensions, while the subsequent ConcatConv2d layer continues to process these features under the same dimensional constraints.

Both models begin with a convolutional layer (Conv2d) that processes a 3-channel input image to produce 32 feature maps using a 3×3 filter with a stride of 2 and padding of 1. The resulting feature maps are then normalized through a Batch Normalization (BN) layer. Following the initial convolutional layer, the features pass through a group of either three ResBlocks or a single ODEBlock, depending on the configuration. Subsequently, the network transitions through a Downsample layer, which effectively reduces the spatial dimensions while adjust the channel depth, preparing the

features for subsequent layers. For instance, after the first group of blocks, a downsample layer increases the channel depth from 32 to 64 while reducing the spatial resolution, preparing the data for the next set of deeper processing layers. Then the feature maps are processed through additional groups of three ResBlocks or an ODEBlock, followed by another downsample layers to transition the channel depth from 64 to 128. After the third group of three ResBlocks or an ODEBlock, the network utilizes an adaptive average pooling layer to condenses the feature maps into a single dimensional vector per feature map. This vector is then flattened and passed through a linear layer which acts as the classifier of the network, outputting the final predictions across the categories.

B Differential Privacy of Gaussian Mechanism

The following result is proved in [20]. Since it is crucial to the results in the body, a slightly different proof is provided here for completeness.

PROPOSITION B.1 (THEOREM A.1 IN [20]). *Let $\epsilon \in (0, 1)$. The Gaussian mechanism, $\mathbf{M}(\mathbf{q}) = \mathbf{f}(\mathbf{q}) + \mathcal{N}(0, \sigma^2 \mathbf{I})$ with variance parameter $\sigma \geq \sqrt{2 \ln(1.25/\delta)}(S_{\mathbf{f}}/\epsilon)$ is (ϵ, δ) -differentially private.*

PROOF. Consider two adjacent datasets \mathbf{q}, \mathbf{q}' , i.e., $|\mathbf{q} - \mathbf{q}'| < 1$. Without loss of generality, write $\mathbf{f}(\mathbf{q}) = \mathbf{f}(\mathbf{q}') + \mathbf{v}$ for some $\mathbf{v} \in \mathbb{R}^n$. Drawing $\mathbf{X} \sim \mathcal{N}(\mathbf{0}, \sigma^2 \mathbf{I})$, the proof is based on analyzing the privacy loss random variable,

$$\begin{aligned} \ln \left(\frac{\Pr[\mathbf{M}(\mathbf{q}) = \mathbf{f}(\mathbf{q}) + \mathbf{X}]}{\Pr[\mathbf{M}(\mathbf{q}') = \mathbf{f}(\mathbf{q}') + \mathbf{X}]} \right) &= \ln \left(\frac{\exp\left(\frac{-1}{2\sigma^2} |\mathbf{X}|^2\right)}{\exp\left(\frac{-1}{2\sigma^2} |\mathbf{X} + \mathbf{v}|^2\right)} \right) \\ &= \frac{1}{2\sigma^2} \left(|\mathbf{X} + \mathbf{v}|^2 - |\mathbf{X}|^2 \right) = \frac{\langle \mathbf{v}, \mathbf{X} \rangle}{\sigma^2} + \frac{|\mathbf{v}|^2}{2\sigma^2}, \end{aligned}$$

which is normally distributed with mean $|\mathbf{v}|^2 / (2\sigma^2)$ and variance $|\mathbf{v}|^2 / \sigma^2$. Choosing $\mathbf{Z} \sim \mathcal{N}(\mathbf{0}, \mathbf{I})$, the privacy loss random variable is bounded by ϵ when

$$\left| \frac{|\mathbf{v}|}{\sigma} \mathbf{Z} + \frac{|\mathbf{v}|^2}{2\sigma^2} \right| \leq \frac{|\mathbf{v}|}{\sigma} \left(|\mathbf{Z}| + \frac{|\mathbf{v}|}{2\sigma} \right) \leq \epsilon.$$

In view of this, it suffices to bound the tail probability

$$\Pr \left[|\mathbf{Z}| > \frac{\epsilon\sigma}{|\mathbf{v}|} - \frac{|\mathbf{v}|}{2\sigma} \right] = 2 \Pr \left[\mathbf{Z} > \frac{\epsilon\sigma}{|\mathbf{v}|} - \frac{|\mathbf{v}|}{2\sigma} \right] < \delta.$$

Choosing the standard deviation $\sigma = t |\mathbf{v}| / \epsilon$ for some $t > 0$ to be determined, Mill's inequality guarantees that it is enough to require

$$\begin{aligned} \Pr \left[\mathbf{Z} > t - \frac{\epsilon}{2t} \right] \\ \leq \frac{1}{\sqrt{2\pi}} \left(t - \frac{\epsilon}{2t} \right)^{-1} \exp \left(-\frac{1}{2} \left(t - \frac{\epsilon}{2t} \right)^2 \right) < \frac{\delta}{2}, \end{aligned}$$

or, said differently, it is enough to choose t such that

$$\ln \left(t - \frac{\epsilon}{2t} \right) + \frac{1}{2} \left(t - \frac{\epsilon}{2t} \right)^2 > \ln \left(\frac{1}{\delta} \sqrt{\frac{2}{\pi}} \right).$$

Note that, by enforcing $t \geq 1$ and $0 < \epsilon < 1$, the first term on the left-hand side is nonnegative when

$$t - \frac{\epsilon}{2t} \geq t - \frac{1}{2} \geq 1,$$

Table 3: Membership inference risks of ODENet-64 models. We evaluate ODENet-64 models against five existing attacks on CIFAR-10 and CIFAR-100. We report the risks based on four different metrics employed in the prior work.

Model	Method	Acc. (C-10)		Acc. (C-100)		TPR @ 0.1% FPR		TPR @ 1% FPR		AUC		Inference acc.	
		Train	Test	Train	Test	C-10	C-100	C-10	C-100	C-10	C-100	C-10	C-100
ODENet-64	Yeom et al. [79]					0.00%	0.03%	0.28%	1.17%	0.536	0.659	53.57%	66.09%
	Shokri et al. [66]					0.08%	0.09%	0.75%	0.85%	0.473	0.480	50.03%	50.01%
	Song and Mittal [68]	94.14%	84.36%	70.93%	51.85%	0.01%	0.13%	0.53%	1.58%	0.511	0.497	51.17%	51.63%
	Watson et al. [73]					0.00%	0.03%	0.28%	1.17%	0.536	0.659	53.57%	66.09%
	Carlini et al. [5]					0.86%	1.72%	4.17%	7.70%	0.639	0.741	59.57%	69.49%

Therefore, it suffices to choose $t \geq 3/2$ to ensure positivity. On the other hand, the second term is increasing in t when $t > \sqrt{\varepsilon/2}$ and decreasing in ε when $\varepsilon < 2t^2$, so it follows that we may ensure

$$\begin{aligned} \left(t - \frac{\varepsilon}{2t}\right)^2 &= t^2 - \varepsilon + \left(\frac{\varepsilon}{2t}\right)^2 \geq t^2 - 1 + 1 \cdot 3^{-2} \\ &= t^2 - \frac{8}{9} > 2 \ln \left(\frac{1}{\delta} \sqrt{\frac{2}{\pi}}\right). \end{aligned}$$

This implies that

$$\begin{aligned} t^2 &> 2 \ln \left(\frac{1}{\delta} \sqrt{\frac{2}{\pi}}\right) + \ln \left(e^{\frac{8}{9}}\right) \\ &= 2 \ln \left(\frac{1}{\delta}\right) + \ln \left(e^{\frac{8}{9}} \frac{2}{\pi}\right), \end{aligned}$$

and since $(2/\pi)e^{8/9} < 1.25^2$, this condition is satisfied when

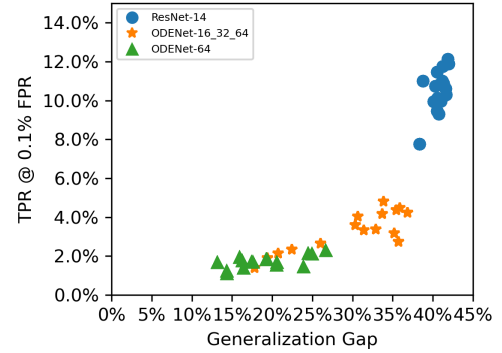
$$t^2 > 2 \ln \left(\frac{1.25}{\delta}\right).$$

This shows that the privacy loss random variable is bounded above by ε with probability $1 - \delta$ on \mathbf{q}, \mathbf{q}' whenever $\sigma \geq \sqrt{2 \ln(1.25/\delta)}$ ($|\mathbf{v}|/\varepsilon$). To remove the dependence on \mathbf{q}, \mathbf{q}' , it suffices to choose $\sigma \geq \sqrt{2 \ln(1.25/\delta)}(S_{\mathcal{F}}/\varepsilon)$. \square

C Additional Evaluation Results

Membership risks of NODEs, based on ODENet-64 architecture. Table 3 and Table 4 summarizes our additional results on NODE (ODENet-64) models and NSDEs with $k = 0$, respectively. It is notable that ODENet-64 demonstrates comparable results to ODENet-16_32_64 but with a decrease in test accuracy of 1.64% and 2.41% on CIFAR-10 and CIFAR-100, respectively. It is $2.5\text{-}6 \times$ less susceptible to LiRA attacks compared to ResNet-14. On CIFAR-100, ODENET exhibits superior defense capabilities against LiRA attacks than ODENET-16_32_64, demonstrating a lower TPR@0.1%FPR of 1.72%, thereby demonstrating enhanced security against membership inference attacks compared to ResNet-14. For NSDEs with $k = 0$, despite being the non-privacy variant, it exhibits robust defense capabilities. NSDEs with $k = 0$ maintains competitive test accuracy and generalization gaps on both CIFAR datasets. Notably, NSDEs $k = 0$ showcases its strengths in defending against membership inference attacks, with TPR@0.1%FPR of 0.35% and 1.03% for CIFAR-10 and CIFAR-100, respectively, demonstrating a stronger defense compared to ResNet-14 and NODE models. This superior performance

in TPR@0.1%FPR, coupled with robust accuracy metrics, underscores NSDE's ability to enhance security against advanced threats.

**Figure 8: Membership risks and overfitting in CIFAR-100.**

LiRA success vs. generalization gap in CIFAR-100. Figure 8 illustrates the relationship between membership risks measured by LiRA and the generalization gap for models trained on CIFAR-100. For ResNet-14, the TPR at 0.1% FPR ranges from 8%–14%, even as the generalization gap remains consistently around 40%. This suggests that overfitting contributes to membership inference risks. In contrast, NODEs (ODENet-16_32_64 and ODENet-64) show slightly lower generalization gaps, typically ranging from 5%–30%. Their TPR at 0.1% FPR values are also lower, fluctuating between 0.5%–5.5%. This suggests that NODEs are less prone to overfitting, thereby reducing their risks to membership inference attacks.

Figure and tables for additional results. Here, we present full experimental results to support the findings reported in the main body of the manuscript: Tables 5–9, where each table covers specific aspects. Table 5 demonstrates the results with varying number of blocks of models in Figure 2 and 6. Table 6 and 7 provide supporting data for Figure 2, illustrating the results of the impact of solvers and variants for NODEs. The detailed evaluation results of defenses, which provide an in-depth analysis corresponding to Figure 3, are presented in Table 8. A complete set of the ablation study regarding the hyperparameters characterizing NSDEs are listed in Table 9, where the subset of it is reported in Figure 6.

Table 4: Membership inference risks of SDENet $\sigma=0$ models. We evaluate SDENet $\sigma=0$ models against five existing attacks on CIFAR-10 and CIFAR-100. We compare their risks based on four different metrics used in the prior work.

Model	Method	Acc. (C-10)		Acc. (C-100)		TPR @ 0.1% FPR		TPR @ 1% FPR		AUC		Inference acc.	
		Train	Test	Train	Test	C-10	C-100	C-10	C-100	C-10	C-100	C-10	C-100
SDENet $\sigma=0$	Yeom et al. [79]					0.00%	0.09%	0.39%	1.12%	0.538	0.625	54.00%	60.52%
	Shokri et al. [66]					0.07%	0.05%	0.68%	0.63%	0.468	0.449	50.02%	50.00%
	Song and Mittal [68]	89.09%	83.93%	68.01%	52.49%	0.00%	0.14%	0.50%	1.40%	0.516	0.496	51.65%	51.13%
	Watson et al. [73]					0.00%	0.09%	0.44%	1.12%	0.538	0.625	54.00%	60.52%
	Carlini et al. [5]					0.35%	1.03%	2.02%	5.36%	0.559	0.676	54.09%	62.26%

Table 5: Comparing membership risks of NODEs and NSDEs. We vary the number of blocks in {1, 2, 3} and use LiRA.

Model	# of Blocks	Acc. (C-10)		Acc. (C-100)		TPR @ 0.1% FPR		TPR @ 1% FPR		AUC		Inference acc.	
		Train	Test	Train	Test	C-10	C-100	C-10	C-100	C-10	C-100	C-10	C-100
ODENet-16_32_64	1	94.30%	84.41%	82.05%	52.16%	1.01%	3.30%	4.22%	12.11%	0.616	0.782	57.65%	72.88%
	2	96.39%	85.26%	93.4%	52.8%	1.57%	7.01%	5.95%	20.86%	0.638	0.848	58.99%	75.77%
	3	96.82%	85.25%	94.71%	53.07%	1.66%	7.78%	6.17%	22.38%	0.641	0.852	58.86%	76.32%
ODENet-64	1	94.14%	84.36%	64.54%	70.93%	0.86%	1.72%	4.17%	7.70%	0.639	0.741	59.57%	69.49%
	2	97.07%	85.20%	80.74%	53.39%	1.25%	2.41%	5.43%	10.59%	0.656	0.788	60.78%	64.33%
	3	97.74%	85.82%	87.26%	53.78%	1.49%	3.29%	6.05%	13.71%	0.669	0.815	60.89%	69.85%
SDENet-16_32_64	1	81.89%	81.91%	56.54%	50.64%	0.14%	0.43%	1.24%	3.00%	0.525	0.612	51.89%	57.64%
	2	82.41%	82.42%	57.2%	51.12%	0.14%	0.45%	1.25%	2.99%	0.528	0.619	52.23%	58.57%
	3	74.44%	74.96%	55.73%	48.27%	0.08%	0.32%	0.90%	2.58%	0.511	0.604	50.00%	57.43%

Table 6: Membership risks of NODEs trained with different solvers. We compare the LiRA success on them.

Model	Solver	Acc. (C-10)		Acc. (C-100)		TPR @ 0.1% FPR		TPR @ 1% FPR		AUC		Inference acc.	
		Train	Test	Train	Test	C-10	C-100	C-10	C-100	C-10	C-100	C-10	C-100
ODENet-16_32_64	Euler	94.30%	84.41%	82.05%	52.16%	1.01%	3.30%	4.22%	12.11%	0.616	0.782	57.65%	72.88%
	Rk4	94.28%	84.39%	83.32%	52.19%	0.89%	3.70%	4.02%	13.07%	0.617	0.792	57.78%	73.05%
	Dopri5	94.41%	84.61%	80.20%	52.20%	0.68%	3.02%	3.40%	11.20%	0.609	0.777	57.43%	64.34%

Table 7: Membership risks of NODE variants. We compare the LiRA success on these models in CIFAR-10.

Model	Acc. (Train)	Acc. (Test)	Train-Test Acc. Gap	TPR @ 0.1% FPR	TPR @ 1% FPR	AUC	Inference acc.
SONODE	92.35%	86.52%	5.9%	0.44%	2.62%	0.585	55.81%
ANODE(+64)	89.09%	85.10%	4.0%	0.35%	2.15%	0.572	55.07%
ANODE(+16)	87.60%	84.62%	3.0%	0.24%	1.76%	0.558	54.10%
HBNODE	84.91%	82.11%	2.8%	0.24%	1.74%	0.545	53.10%
ODENet-64 (Baseline)	94.14%	84.36%	9.7%	0.86%	4.17%	0.639	59.57%

Table 8: Effectiveness of defenses in CIFAR-10. We use LiRA. All defenses, except for SDENets, are applied to ResNet-14..

Model	Acc. (Train)	Acc. (Test)	Train-Test Acc. Gap	TPR @ 0.1% FPR	TPR @ 1% FPR	AUC	Inference acc.
Memguard	98.14%	85.97%	12.17%	0.00%	0.00%	0.580	54.48%
MMD+mix-up	95.10%	87.39%	7.71%	2.03%	7.09%	0.628	57.95%
L2-Regularization	98.84%	86.60%	12.24%	2.36%	7.81%	0.675	61.54%
L1-Regularization	97.39%	86.48%	10.91%	1.06%	4.77%	0.641	59.47%
DP-SGD, $\epsilon=8$	73.49%	74.44%	-0.95%	0.12%	1.18%	0.516	51.28%
ResNet-14	98.14%	85.97%	12.17%	3.96%	10.57%	0.679	61.15%
SDENet $\sigma=0$	89.09%	83.93%	5.16%	0.35%	2.02%	0.559	54.09%
SDENet $\sigma=2$	81.89%	81.91%	-0.02%	0.14%	1.24%	0.525	51.89%

Table 9: Full evaluation results of different NSDE configurations.

Impact	Step_size	Time	Stochasticity	Noise	Train Acc.	Test Acc.	TPR @ 0.1% FPR	TPR @ 1% FPR	AUC	Inference acc.
Step_size	8	1	0.5	1.4	83.27%	82.38%	0.15%	1.37%	0.527	52.04%
	16	1	0.5	2	81.89%	81.91%	0.14%	1.24%	0.525	51.89%
	32	1	0.5	2.8	46.65%	35.86%	0.14%	1.29%	0.523	52.10%
Step_size	8	0.5	0.5	2	83.09%	82.52%	0.14%	1.27%	0.527	51.60%
	16	0.5	0.5	2.8	81.61%	82.00%	0.15%	1.26%	0.527	51.99%
	32	0.5	0.5	4	79.26%	80.92%	0.14%	1.15%	0.519	51.37%
Step_size	8	0.25	0.5	2.8	82.40%	82.05%	0.16%	1.27%	0.525	51.88%
	16	0.25	0.5	4	80.89%	81.21%	0.13%	1.20%	0.521	51.59%
	32	0.25	0.5	5.7	77.90%	80.12%	0.12%	1.19%	0.514	50.84%
Step_size	8	0.125	0.5	4	80.61%	80.77%	0.14%	1.26%	0.522	51.49%
	16	0.125	0.5	5.7	78.52%	79.66%	0.14%	1.18%	0.514	51.88%
	32	0.125	0.5	8	75.01%	77.43%	0.11%	1.06%	0.507	50.41%
Step_size	8	1	0.71	2	81.66%	81.96%	0.17%	1.34%	0.524	51.67%
	16	1	0.5	2	81.89%	81.91%	0.14%	1.24%	0.525	51.89%
	32	1	0.35	2	81.64%	82.02%	0.15%	1.31%	0.527	51.78%
Step_size	8	0.5	0.5	2	83.09%	82.52%	0.14%	1.27%	0.527	51.60%
	16	0.5	0.35	2	83.09%	82.50%	0.14%	1.25%	0.528	52.25%
	32	0.5	0.25	2	82.98%	82.32%	0.14%	1.30%	0.530	52.03%
Step_size	8	0.25	0.35	2	83.70%	82.46%	0.15%	1.26%	0.528	52.17%
	16	0.25	0.25	2	83.53%	82.49%	0.18%	1.33%	0.529	52.71%
	32	0.25	0.18	2	83.44%	82.52%	0.17%	1.32%	0.524	51.67%
Step_size	8	0.125	0.25	2	82.98%	81.95%	0.16%	1.29%	0.525	52.34%
	16	0.125	0.18	2	82.91%	81.71%	0.17%	1.28%	0.527	51.55%
	32	0.125	0.13	2	82.88%	81.70%	0.17%	1.36%	0.526	52.34%
Time	8	1	0.5	1.4	83.27%	82.38%	0.15%	1.37%	0.528	52.04%
	8	0.5	0.5	2	83.09%	82.52%	0.14%	1.27%	0.527	51.60%
	8	0.25	0.5	2.8	82.40%	82.05%	0.16%	1.27%	0.525	51.88%
	8	0.125	0.5	4	80.61%	80.77%	0.14%	1.26%	0.523	51.49%
Time	16	1	0.5	2	81.89%	81.91%	0.14%	1.24%	0.525	51.89%
	16	0.5	0.5	2.8	81.61%	82.00%	0.15%	1.26%	0.527	51.99%
	16	0.25	0.5	4	80.89%	81.21%	0.13%	1.20%	0.521	51.59%
	16	0.125	0.5	5.7	78.52%	79.66%	0.14%	1.18%	0.514	51.88%
Time	32	1	0.5	2.8	46.65%	35.86%	0.14%	1.29%	0.523	52.10%
	32	0.5	0.5	4	79.26%	80.92%	0.14%	1.15%	0.519	51.37%
	32	0.25	0.5	5.7	77.90%	80.12%	0.12%	1.19%	0.514	50.84%
	32	0.125	0.5	8	74.60%	77.22%	0.12%	1.01%	0.510	50.14%
Time	8	1	0.71	2	81.66%	81.96%	0.17%	1.34%	0.524	51.67%
	8	0.5	0.5	2	83.09%	82.52%	0.14%	1.27%	0.527	51.60%
	8	0.25	0.35	2	83.70%	82.46%	0.15%	1.26%	0.528	52.17%
	8	0.125	0.25	2	82.98%	81.95%	0.16%	1.29%	0.525	52.34%
Time	16	1	0.5	2	81.89%	81.91%	0.14%	1.24%	0.525	51.89%
	16	0.5	0.35	2	83.09%	82.50%	0.14%	1.25%	0.523	52.25%
	16	0.25	0.25	2	83.53%	82.49%	0.18%	1.33%	0.529	52.71%
	16	0.125	0.18	2	82.91%	81.71%	0.17%	1.28%	0.527	51.6%
Time	32	1	0.35	2	81.64%	82.02%	0.15%	1.31%	0.527	51.78%
	32	0.5	0.25	2	82.98%	82.32%	0.14%	1.30%	0.530	52.03%
	32	0.25	0.18	2	83.44%	82.52%	0.17%	1.32%	0.524	51.67%
	32	0.125	0.13	2	82.88%	81.70%	0.17%	1.36%	0.526	52.34%
k	16	1	0.3	1.2	83.56%	82.62%	0.15%	1.29%	0.530	51.29%
	8	1	0.5	1.4	82.38%	82.38%	0.15%	1.37%	0.528	52.04%
	16	1	0.4	1.6	82.58%	82.22%	0.17%	1.40%	0.528	52.27%
	8	0.5	0.5	2	83.09%	82.52%	0.14%	1.27%	0.527	51.60%
	16	1	0.6	2.4	63.23%	57.12%	0.09%	1.09%	0.516	52.02%
	8	0.25	0.5	2.8	82.40%	82.05%	0.16%	1.27%	0.525	51.88%
	16	0.25	0.5	4	80.89%	81.21%	0.13%	1.20%	0.521	51.59%
	32	0.25	0.5	5.7	77.90%	80.12%	0.12%	1.19%	0.514	50.84%
Stochasticity	0.3	1	16	1.2	83.56%	82.62%	0.15%	1.29%	0.516	52.02%
	0.4	1	16	1.6	82.58%	82.22%	0.17%	1.40%	0.528	52.27%
	0.5	1	16	2	81.89%	81.91%	0.14%	1.24%	0.525	51.89%
	0.6	1	16	2.4	63.23%	57.12%	0.09%	1.09%	0.516	52.02%